Myo1c binding to submembrane actin mediates insulin-induced tethering of GLUT4 vesicles

Shlomit Boguslavsky[a], Tim Chiu[a], Kevin P. Foley[a], Cesar Osorio-Fuentealba[a,b], Costin N. Antonescu[c], K. Ulrich Bayer[d], Philip J. Bilan[a], and Amira Klip[a]

[a]Cell Biology Program, Hospital for Sick Children, Toronto, ON M5G 1X8, Canada; [b]FONDAP-CEMC Instituto de Ciencias Biomedicas, University of Chile, Santiago 6530499, Chile; [c]Department of Chemistry and Biology, Ryerson University, Toronto, ON M5B 2K3, Canada; [d]Department of Pharmacology, University of Colorado Denver–School of Medicine, Aurora, CO 80045-0508

ABSTRACT **GLUT4-containing vesicles cycle between the plasma membrane and intracellular compartments. Insulin promotes GLUT4 exocytosis by regulating GLUT4 vesicle arrival at the cell periphery and its subsequent tethering, docking, and fusion with the plasma membrane. The molecular machinery involved in GLUT4 vesicle tethering is unknown. We show here that Myo1c, an actin-based motor protein that associates with membranes and actin filaments, is required for insulin-induced vesicle tethering in muscle cells. Myo1c was found to associate with both mobile and tethered GLUT4 vesicles and to be required for vesicle capture in the total internal reflection fluorescence (TIRF) zone beneath the plasma membrane. Myo1c knockdown or overexpression of an actin binding–deficient Myo1c mutant abolished insulin-induced vesicle immobilization, increased GLUT4 vesicle velocity in the TIRF zone, and prevented their externalization. Conversely, Myo1c overexpression immobilized GLUT4 vesicles in the TIRF zone and promoted insulin-induced GLUT4 exposure to the extracellular milieu. Myo1c also contributed to insulin-dependent actin filament remodeling. Thus we propose that interaction of vesicular Myo1c with cortical actin filaments is required for insulin-mediated tethering of GLUT4 vesicles and for efficient GLUT4 surface delivery in muscle cells.**

Monitoring Editor
Laurent Blanchoin
CEA Grenoble

Received: Apr 5, 2012
Revised: Jul 19, 2012
Accepted: Aug 16, 2012

INTRODUCTION

Actin filaments are fundamental elements in intracellular vesicle traffic (Ridley, 2006; Lanzetti, 2007), in part through their continuous assembly and disassembly (i.e., actin remodeling; Blanchoin *et al.*, 2000; Pollard, 2007). Actin dynamics is required for budding, fission, and transport of Golgi carriers (Egea *et al.*, 2006), and cortical actin remodeling beneath the plasma membrane is required for efficient endocytic and exocytic events at the plasma membrane (Lanzetti, 2007). Actin filament dynamics is also notably involved in the insulin-dependent translocation of glucose transporter GLUT4 to the membranes of muscle and fat cells (Tsakiridis *et al.*, 1994; Kanzaki and Pessin, 2001; Tong *et al.*, 2001; Lopez *et al.*, 2009; Chiu *et al.*, 2011b; Stockli *et al.*, 2012). Insulin-dependent GLUT4 translocation is the rate-limiting step in the capture of glucose, a phenomenon particularly important in skeletal muscle, as this is the primary tissue responsible for dietary glucose disposal.

GLUT4-containing vesicles continuously cycle between the plasma membrane and several intracellular compartments (e.g., endosomes, *trans*-Golgi network), and insulin promotes GLUT4 vesicle exocytosis (Dugani and Klip, 2005). Extensive research shows that insulin-induced intracellular signals regulate the arrival, tethering, docking, and fusion of GLUT4 vesicles with the membrane (reviewed by Foley *et al.*, 2011; Stockli *et al.*, 2012). Whereas docking and fusion are mediated by a subset of soluble *N*-ethylmaleimide–sensitive factor attachment protein receptor (SNARE) proteins (Foster and Klip, 2000; Watson and Pessin, 2007; Zaid *et al.*, 2008; Stockli *et al.*,

This article was published online ahead of print in MBoC in Press (http://www.molbiolcell.org/cgi/doi/10.1091/mbc.E12-04-0263) on August 23, 2012.

Address correspondence to: Amira Klip (amira@sickkids.ca).

Abbreviations used: BSA, bovine serum albumin; CaMKII, Ca^{2+}- and calmodulin-dependent kinase II; FBE, filament barbed ends; FDB, *flexor digitorum brevis*; FITC, fluorescein isothiocyanate; GFP, green fluorescent protein; HA, hemagglutinin; NA, numerical aperture; PBS, phosphate-buffered saline; PFA, paraformaldehyde; RFP, red fluorescent protein; ROI, region of interest; siNR, nonrelated, control siRNA; siRNA, small interfering RNA; SNARE, soluble *N*-ethylmaleimide–sensitive factor attachment protein receptor; T, truncated; TIRF, total internal reflection fluorescence; WT L6, wild-type L6; YFP, yellow fluorescent protein.

2012), the molecular machinery involved in GLUT4 vesicle tethering is unknown (Stockli *et al.*, 2012).

Efficient GLUT4 translocation is the result of exquisite coordination of signal transduction with elaborate membrane plasticity, along with the participation of actin dynamics (Zaid *et al.*, 2008; Chiu *et al.*, 2011a; Foley *et al.*, 2011; Stockli *et al.*, 2012). Indeed, in muscle and fat cells in culture and in mature skeletal muscle and primary adipocytes, insulin induces robust actin remodeling, supporting membrane ruffles at the cell periphery (Khayat *et al.*, 2000; Kanzaki and Pessin, 2001; Tong *et al.*, 2001; Brozinick *et al.*, 2004; JeBailey *et al.*, 2004, 2007). Preventing actin remodeling with latrunculin B or cytochalasin D (Tsakiridis *et al.*, 1994; Lopez *et al.*, 2009) or stabilizing preexisting actin filaments with jasplakinolide (Kanzaki and Pessin, 2001; Tong *et al.*, 2001) each precludes GLUT4 translocation, yet there is no consensus on the steps that involve actin dynamics. In adipocytes, interfering with actin polymerization impairs the final exocytic fusion step (Lopez *et al.*, 2009), whereas in muscle cells it prevents the availability of GLUT4 near the cell periphery (Randhawa *et al.*, 2008). In either cell type, the precise molecular events governed by actin filaments are unknown.

Actin filaments might serve as tracks for processive movement of GLUT4 vesicles, or alternatively, they may gather vesicles in an "active zone" beneath the plasma membrane for subsequent fusion. Both functions may depend on actin-associated molecular motors of the myosin family. Indeed, on one hand, members of the myosin V family that advance along actin as processive motors have been implicated in the translocation of GLUT4 to the plasma membrane in muscle and fat cells (Yoshizaki *et al.*, 2007; Ishikura and Klip, 2008). On the other hand, the nonprocessive, class 1 myosin Myo1c (Loubery and Coudrier, 2008) was recently found to be necessary for insulin-dependent glucose uptake in skeletal muscle (Toyoda *et al.*, 2011), and its down-regulation reduces insulin-dependent GLUT4 translocation in 3T3-L1 adipocytes (Bose *et al.*, 2002, 2004). Class 1 myosins are particularly interesting, since they can simultaneously associate with membranes and actin filaments (Adams and Pollard, 1989; Tang *et al.*, 2002; McKenna and Ostap, 2009), thereby regulating membrane–cytoskeleton adhesion (Nambiar *et al.*, 2009). Accordingly, they participate in endocytosis, exocytosis, and regulation of tension between the cytoskeleton and the plasma membrane (McConnell and Tyska, 2010). Myo1c induces actin filament remodeling via its association with Rictor, independently of insulin input (Hagan *et al.*, 2008), and it has also been proposed that Ca^{2+}- and calmodulin-dependent kinase II (CaMKII) directly phosphorylates and activates the ATPase activity of Myo1c in insulin-stimulated adipocytes (Yip *et al.*, 2008). However, the molecular mechanism whereby Myo1c regulates GLUT4 remains poorly understood, and it is unknown whether it participates at all in GLUT4 traffic in muscle cells.

In this paper, we report that Myo1c in muscle cells associates with dynamic GLUT4 vesicles that move along linear paths in the total internal reflection fluorescence (TIRF) zone beneath the membrane and reduces GLUT4 vesicle velocity. Insulin causes immobilization of GLUT4-positive vesicles underneath the plasma membrane, and this immobilization is dependent on the presence of Myo1c and its actin-binding activity. While insulin stimulation activated CaMKII, extensive tests did not reveal involvement of this enzyme in GLUT4 surface delivery. We conclude that binding of vesicle-bound Myo1c to actin filaments underlies its participation in GLUT4 tethering within the TIRF zone for subsequent productive docking and fusion of GLUT4 vesicles with the muscle cell membrane.

RESULTS

Myo1c and GLUT4 associate and colocalize in submembrane vesicles and membrane ruffles

Myo1c is expressed in L6 myoblasts and myotubes and in mouse skeletal muscle (Supplemental Figure 1, A and B). Stably or transiently transfected GLUT4*myc* responds to insulin in myoblasts and myotubes with a greater than twofold gain at the cell surface, akin to the changes observed in mature skeletal muscle (Zaid *et al.*, 2008). The myoblast stage affords a useful and well-characterized system to study the cell biology of GLUT4 traffic and its regulation by insulin in a muscle cell background (Ueyama *et al.*, 1999). Insulin (100 nM, 20 min) caused enrichment in GLUT4*myc* at ruffled membrane areas (as reported earlier in Tong *et al.*, 2001) and endogenous Myo1c colocalized with stably transfected GLUT4*myc* at these sites (Figure 1A; top panels show collapsed (compressed) focal planes, bottom panels show single focal plane). This finding is in agreement with the colocalization of the two proteins at the plasma membrane of 3T3-L1 adipocytes (Bose *et al.*, 2004). The insulin-dependent Myo1c accumulation at sites of actin remodeling was not due to the accumulation of membrane area in them, since the ratio of endogenous Myo1c to concanavalin A (plasma membrane glycoprotein ligand) in the ruffled areas increased (Figure S1C). Myo1c was not found at perinuclear regions rich in GLUT4.

Myo1c and GLUT4*myc* colocalized in vesicular structures in the TIRF zone, whose dynamic behavior was examined in live myoblasts. Any puncta that were positive for GLUT4*myc*–green fluorescent protein (GFP) and that appeared spherical in shape, stood alone, and were clearly discernible from neighboring structures were considered "GLUT4 vesicles." Examples of these had a median fluorescence intensity 3.1-fold above background and appeared as single diffraction-limited structures (Figure S2, A and B; $n = 67$ structures), detected by analysis of manually selected structures as described in Thomann *et al.* (2002). Such structures (termed here *vesicles*) were then selected for further analysis. Cotransfected GLUT4*myc*–red fluorescent protein fusion protein (GLUT4-RFP) and Myo1c-yellow fluorescent protein chimera (Myo1c-YFP) colocalized in both bidirectionally moving (Figure 1B, arrowheads) and stationary vesicular structures (Figure 1B, asterisks, and Supplemental Movie S1, a–c). The stationary vesicles exhibited no apparent change in their lateral position or intensity for at least 5 s, whereas mobile vesicles exhibited lateral displacements or changed their intensity due to vertical displacement in the TIRF zone (Movie S1, a–c). Within the mobile population, two types of lateral motion were detected in the time frame imaged: short-range vibrations (ranging between 0.1–3.0 μm) and short- and long-range, linear displacements of up to 10 μm.

To examine whether colocalization might have arisen as a result of Myo1c overexpression, we looked at the relative distribution of endogenous Myo1c and transiently transfected GLUT4*myc*-GFP (Figure 1C). Analysis of at least 15 cells per condition again revealed a colocalization between vesicular GLUT4 and endogenous Myo1c in the TIRF zone ($r_{basal} = 0.64 \pm 0.06$, $p < 0.05$), where r is the Pearson's coefficient. Insulin did not significantly change the degree of colocalization ($r_{insulin} = 0.7 \pm 0.03$, $p < 0.05$).

A connection between GLUT4 and Myo1c was further made evident by the ability of the two proteins to coimmunoprecipitate. Anti-*myc* antibody-bound Sepharose beads were used to immunoprecipitate GLUT4*myc* from lysates of L6 myoblasts stably expressing GLUT4*myc* (L6-GLUT4*myc* cells) so as not to interfere with cytosolic regions of the transporter. Endogenous Myo1c coprecipitated with GLUT4*myc* but was absent in control immunoprecipitates from lysates of untransfected wild-type L6 (WT L6) cells (Figure 1D). Acute prestimulation of cells with insulin did not change the extent of

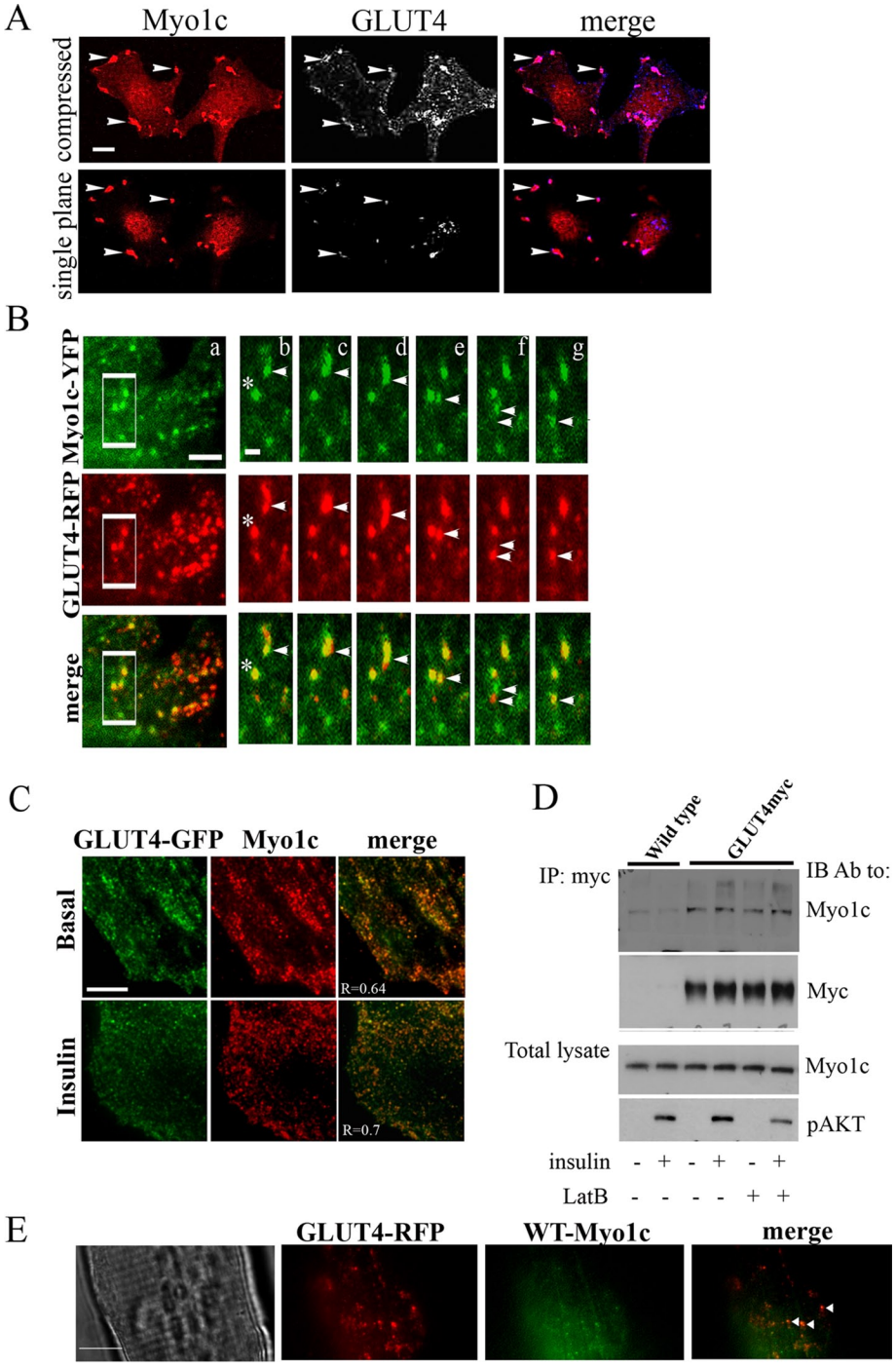

FIGURE 1: Myo1c and GLUT4 colocalize at the plasma membrane and on mobile intracellular vesicles. (A) Myo1c colocalizes with surface GLUT4 in insulin-induced ruffles. L6-GLUT4*myc* myoblasts were treated with insulin (100 nM, 10 min). Surface-localized GLUT4*myc* was labeled with anti-*myc* prior to permeabilization and Myo1c was then labeled after permeabilization. Shown are representative confocal images (of three experiments) acquired from a single focal plane 4–6 µm above the coverslip (to capture insulin-induced ruffles that may protrude 2–3 µm above the dorsal focal plane of the cell) and a combined image (compressed) of all focal planes. Arrowheads indicate Myo1c and GLUT4 sites of colocalization. In the merged image, blue artificial color represents GLUT4 staining. Scale bar: 10 µm. (B) Myo1c localizes to dynamic vesicles and colocalizes with GLUT4-positive vesicles at the TIRF zone. WT L6 myoblasts were transiently cotransfected with GLUT4-RFP (shown in red) and Myo1c-YFP (shown in green), incubated in serum-free media for 3 h, and imaged live using multicolor TIRF microscopy (Movie S1, a–c). Panel (a) shows a single frame of a representative cell in the basal state. The outlined region in panel (a) is magnified in panels (b–g), which are individual frames of this region captured 2-s apart. One stationary vesicle in which the two proteins colocalize is marked by an asterisk. Instances of colocalization on mobile vesicles are indicated by arrowheads. Scale bars: 5 and 0.8 µm (insets). (C) Endogenous Myo1c (red) colocalizes with GLUT4-GFP (green) vesicles. WT L6 myoblasts were transfected with GLUT4-GFP and treated without/with insulin as in (A); this was followed by immunofluorescence labeling of endogenous Myo1c and then multicolor TIRF microscopy imaging of fixed cells. The extent of colocalization was quantified using the Pearson's *r* (*R*) as described in *Materials and Methods*. Scale bar: 5 µm. (D) Endogenous Myo1c coimmunoprecipitates with GLUT4. Lysates of serum-starved L6-GLUT4*myc* or WT L6 myoblasts were pretreated with/without 1 µM latrunculin B (LatB) for 1 h; this was followed by insulin stimulation as in (A). GLUT4 immunoprecipitates (IP) were immunoblotted (IB) with Myo1c antibody or anti-Myc antibody (GLUT4*myc*). Shown is one representative blot out of three independent experiments. (E) Unstimulated FDB fibers expressing GLUT4-RFP and WT-Myo1c-YFP were fixed but not permeabilized. A representative TIRF image from three independent experiments is illustrated in differential image contrast (DIC), red and green channels, and as a merged image. Arrowheads mark the colocalization of the two proteins on punctate vesicular structures in the submembrane region of the muscle fiber. Scale bar: 100 µm.

coprecipitation of Myo1c with GLUT4*myc*. The interaction between the two proteins was preserved in the presence of a high concentration of the actin-depolymerizing agent latrunculin B, indicating that their association is not mediated by actin filaments (Figure 1D). We also assessed the colocalization of Myo1c and GLUT4 in vesicular structures in isolated *flexor digitorum brevis* (FDB) skeletal muscle fibers. Firstly, FDB muscle fibers were cotransfected by electroporation with plasmid DNA constructs for WT-Myo1c-YFP and GLUT4-RFP and analyzed 10 d posttransfection for colocalization using two-color TIRF microscopy (Figure 1E). Analysis of at least 15 different FDB fibers from three different animals revealed that WT-Myo1c-YFP colocalized with GLUT4-RFP in many vesicular puncta (Figure 1E). In addition, FDB muscle fibers transfected with GLUT4-RFP alone were processed by indirect immunofluorescence using epifluorescence microscopy to detect endogenous Myo1c. Analysis of at least 15 muscle fibers showed colocalization of endogenous Myo1c with GLUT4-RFP–positive vesicles (unpublished data). Together the results in Figure 1 indicate that Myo1c binds to and colocalizes with GLUT4 on mobile and immobile vesicles and that

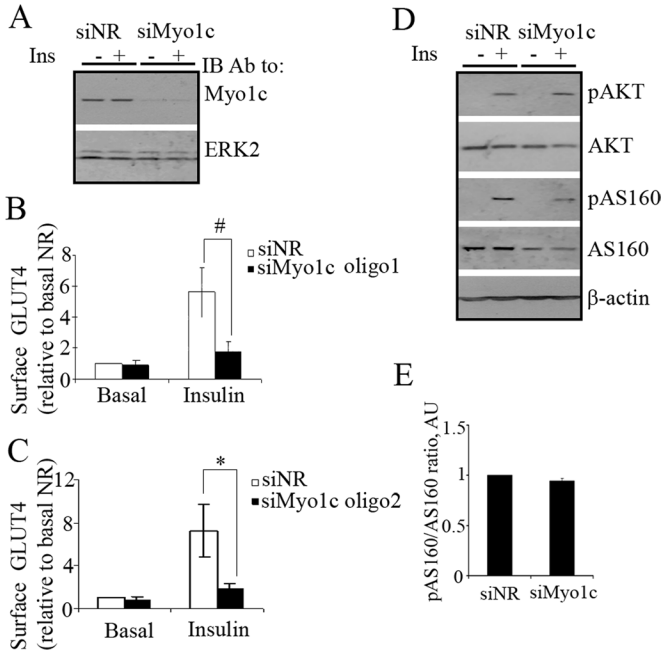

FIGURE 2: Insulin-stimulated GLUT4 translocation to the plasma membrane is reduced by Myo1c knockdown. (A) Efficient siRNA-mediated knockdown of Myo1c (200 nM, oligo 1) as indicated by immunoblotting. siNR was used as a negative control, and expression of ERK was not affected. Shown is one representative blot out of three independent experiments. L6-GLUT4*myc* myoblasts were transfected with siNR or Myo1c siRNA (siMyo1c) and treated with/without insulin as in Figure 1. (B and C) WT L6 myoblasts transfected with siNR or siMyo1c oligo 1 (B, $n = 4$) or oligo 2 (C, $n = 2$), were transiently transfected with GLUT4*myc*-GFP. Forty-eight hours after transfection, the cells were treated with/without insulin; this was followed by staining of surface GLUT4*myc* and endogenous Myo1c as in Figure 1B. Knockdown cells with low expression of Myo1c were further analyzed for surface GLUT4 fluorescence intensity (at least 20 cells per condition). Quantification of fold increases in surface GLUT4*myc* relative to the siNR basal is presented (mean ± SE, #, $p < 0.05$, *, $p = 0.08$). (D) L6-GLUT4*myc* myoblasts stably expressing AS160 were transfected with siNR or siMyo1c and treated with/without insulin as above. Shown is one representative immunoblot for native and phospho-Akt and phospho-AS160 out of three independent experiments. (E) The pAS160/AS160 ratio from (D) is calculated from three independent experiments.

both proteins accumulate together at membrane ruffles in response to insulin.

Myo1c knockdown reduces insulin-stimulated gain in surface GLUT4

To determine the functional relevance of Myo1c to insulin-induced GLUT4 traffic in muscle cells, we used targeted small interfering RNA (siRNA)-mediated Myo1c gene silencing. Treatment of myoblasts with siMyo1c achieved 75 ± 3% knockdown (Figure 2A) relative to treatment with nonrelated, control siRNA (siNR). Myo1c knockdown did not significantly alter the basal-state level of surface GLUT4*myc*, but it markedly inhibited the insulin-induced gain by 70% (Figure 2B). The selectivity of siMyo1c for insulin-dependent GLUT4*myc* translocation was confirmed using a second oligonucleotide targeting a different sequence in the Myo1c transcript, which achieved an 80% knockdown (not illustrated) and reduced GLUT4*myc* translocation by 75% (Figure 2C). Of note, down-regulation of Myo1c did not reduce the recycling of fluorescently labeled transferrin (Figure S3) in insulin-stimulated cells, suggesting that the effect on insulin-dependent GLUT4 exocytosis is specific. In unstimulated cells depleted of Myo1c, there was a trend to reduce transferrin recycling that was not statistically significant (Figure S3).

To exclude any possible effect of Myo1c knockdown on upstream insulin signaling, we analyzed insulin-stimulated phosphorylation of Akt and of its substrate AS160. Myo1c knockdown did not perturb Akt phosphorylation on Ser473, however AS160 expression was mildly reduced, with a consequent decrease in Thr642-AS160 phosphorylation (Figure 2D), thereby maintaining the ratio of phospho-AS160 to total AS160 (Figure 2E). The decrease in AS160 expression is likely inconsequential to GLUT4 traffic, because strong siRNA-mediated knockdown of this protein increases the basal levels of surface GLUT4 (Ishikura *et al.*, 2008; Brewer *et al.*, 2011), yet the mild reduction in AS160 caused by siMyo1c did not alter the basal levels of surface GLUT4. In contrast, as shown above, siMyo1c knockdown virtually abolished GLUT4 translocation. These results indicate that the effect of Myo1c ablation on the insulin-dependent gain in surface GLUT4 is independent of effects on insulin signaling at the levels of Akt and AS160.

Myo1c is not required for cytosolic dispersion of perinuclear GLUT4

Given that Myo1c is required for the insulin-dependent gain in surface GLUT4, we asked whether it participates in the insulin-dependent movement of GLUT4 from the perinuclear region to the cell periphery (i.e., GLUT4 cytosolic dispersion) or whether it affects GLUT4 vesicles at the vicinity of the plasma membrane. GLUT4accumulates in tubulo-vesicular structures at a perinuclear pole only partly overlapping with the transferrin receptor, giantin, and furin (respective markers of the recycling vesicles, Golgi complex, and *trans*-Golgi network), and insulin causes dispersion of perinuclear GLUT4 toward the cell periphery (Dugani *et al.*, 2008). We silenced expression of Myo1c and examined the insulin-dependent perinuclear-to-cytosolic dispersion of GLUT4*myc*-GFP transiently transfected in WT L6 myoblasts. GLUT4*myc*-GFP distribution was analyzed by counting the number of cells in which the vast majority of GLUT4*myc*-GFP concentrated at the perinuclear region (Figure 3A, left panel) and the number of cells with the majority of GLUT4 dispersed in the cytosol (Figure 3A, right panel). Only cells with low expression of GLUT4*myc*-GFP were selected for analysis. As expected, insulin stimulation caused a significant increase in the percentage of cells with cytosolic GLUT4*myc*-GFP in control siNR cells (basal 19 ± 9% vs. insulin 62 ± 5%, $p < 0.05$; Figure 3B). This behavior was not altered in Myo1c knockdown cells (basal 15 ± 4%, insulin 52% ± 4%, $p < 0.05$; Figure 3B). In contrast, down-regulation of a different motor protein also implicated in insulin-stimulated GLUT4 translocation, MyoIIA (Chung Le *et al.*, 2009; and our unpublished data), caused a significant decrease in the percentage of cells with insulin-induced cytosolic dispersion of GLUT4*myc*-GFP (basal 14 ± 10%, insulin 36 ± 11%, $p < 0.05$; Figure 3C). These results suggest that unlike MyoIIA, Myo1c is not required for the insulin-stimulated redistribution of perinuclear GLUT4 to the cytosol.

Myo1c is required for GLUT4 capture at the TIRF zone

Because loss of Myo1c did not affect cytosolic dispersion of GLUT4 vesicles but prevented exposure of GLUT4 to the extracellular medium, we inquired whether instead Myo1c affects GLUT4 vesicle accumulation beneath the plasma membrane. L6 myoblasts were cotransfected with siNR or siMyo1c along with GLUT4*myc*-GFP, fixed, permeabilized, and labeled with anti-Myo1c antibody.

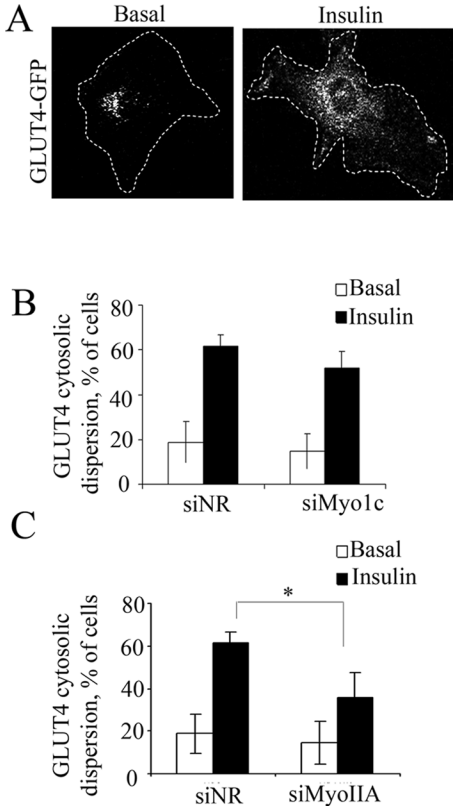

FIGURE 3: Myo1c is not required for cytosolic dispersion of GLUT4 to the cell periphery. (A) Representative images of the typical perinuclear localization of GLUT4*myc*-GFP in basal (left) and cytosolic localization in the insulin-stimulated state (right). (B and C) WT L6 myoblasts transfected with siNR, siMyo1c (B), or siMyoIIA (C), were transiently transfected with GLUT4*myc*-GFP. After 24 h, cells were transferred to glass coverslips and allowed to recover for 24–48 h. Cells were then treated with/without insulin for 20 min; this was followed by staining of endogenous Myo1c (B, $n = 4$) or MyoIIA (C, $n = 3$). Knockdown cells (at least 20 cells per condition) with low expression of Myo1c (B) or MyoIIA (C) were selected for further analysis of the percent of cells with cytosolic dispersion of GLUT4*myc*-GFP (mean ± SD, *, $p < 0.01$) as described in *Materials and Methods*.

Images of fixed, GLUT4*myc*-GFP–positive cells expressing normal (control) or low Myo1c levels (knockdown) were acquired using multicolor TIRF microscopy. Myo1c knockdown caused a small but significant 22.1 ± 1.5% drop ($p < 0.005$) in the number of GLUT4-positive vesicles at the TIRF zone ($n = 25$ for each condition). This suggests that Myo1c is required to capture GLUT4 vesicles at the vicinity of the plasma membrane in unstimulated cells. The effect of insulin on GLUT4 vesicle numbers in the TIRF zone was then analyzed in live cells. WT L6 cells cotransfected with GLUT4-RFP and fluorescently tagged siNR (control) or siMyo1c were imaged live before and after insulin stimulation. In siNR-transfected cells, insulin caused a 54.0 ± 3.5% decrease in the number of GLUT4-RFP vesicles in the TIRF zone relative to the basal condition ($n = 6$, 6–8 regions of interest [ROI] per cell; Figure S2B). This reduction is likely due to consumption of GLUT4 vesicles upon fusion with the plasma membrane, given the insulin-induced increase in surface-exposed GLUT4*myc*. The insulin-dependent loss of GLUT4 vesicles from the TIRF zone was greatly attenuated in cells depleted of Myo1c, which instead exhibited only a 29 ± 9% drop in GLUT4 vesicle number in response to insulin relative to the basal condition ($n = 4$, 6–8 ROI/cell; Figure S2B). Because the number of vesicles was already reduced by Myo1c depletion prior to insulin stimulation, this finding suggests that proper capture of GLUT4 vesicles in the vicinity of the plasma membrane is a necessary preamble for efficient insulin action.

A previous study reported that Myo1c regulates compensatory endocytosis following regulated exocytosis of cortical granules in *Xenopus* eggs (Sokac *et al.*, 2006). To examine whether the insulin-stimulated increase in surface GLUT4 may result from a contribution of Myo1c to GLUT4 endocytosis, we quantified the effect of Myo1c knockdown on GLUT4 internalization. The results revealed that Myo1 depletion did not alter the rate of GLUT4*myc* internalization, which was, however, reduced by silencing expression of clathrin heavy chain, used as control (Figure 4A). In muscle cells, GLUT4 internalizes via clathrin- and clathrin-independent pathways, both requiring dynamin-2 (Antonescu *et al.*, 2008). To further explore whether GLUT4*myc* vesicles colocalizing with Myo1c are exocytic or endocytic, we examined the colocalization of vesicular GLUT4*myc* with endogenous Myo1c upon inhibition of GLUT4 internalization by the inactive mutant of dynamin-2, Dyn2-K44A, which cannot hydrolyze GTP (Cao *et al.*, 2000). Expression of this mutant, which blocks GLUT4 internalization (Antonescu *et al.*, 2008) did not prevent the colocalization of Myo1c with GLUT4*myc*-GFP in the TIRF zone (Figure 4B). While this mutant reduced the number of GLUT-4*myc*-positive vesicles in the TIRF zone, those remaining were still Myo1c-positive in either basal (Figure 4B, left panel) or insulin-stimulated (Figure 4B, right panel) conditions. Together, these data support the scenario that Myo1c impacts predominantly on the exocytic arm of GLUT4 traffic to the cell membrane. Consistent with this scenario, VAMP2, a component of exocytic GLUT4 vesicles (Ramm *et al.*, 2000; Randhawa *et al.*, 2004; Williams and Pessin, 2008; Bogan and Kandror, 2010; Xu *et al.*, 2011), also colocalized with vesicular endogenous Myo1c (Figure S4). Finally, and further supporting the presence of Myo1c in exocytic GLUT4*myc* vesicles, we observed Myo1c on GLUT4*myc* puncta that subsequently underwent fusion with the cell membrane (Figure 4C and Supplemental Movie S2, a–c). Collectively these observations suggest that Myo1c associates with exocytic GLUT4 vesicles in the TIRF zone and is not required for GLUT4 internalization.

We next investigated whether Myo1c is required for the dynamic behavior of GLUT4 vesicles in response to insulin. WT L6 cells cotransfected with GLUT4-RFP and fluorescently tagged siNR or Myo1c siRNA. GLUT4 vesicle velocity was analyzed by TIRF microscopy of live cells before and after insulin stimulation. Three populations of GLUT4 vesicles were identified: 1) vesicles moving at < 0.1 μm/s, which showed no motion within the resolution of our detection (hereafter referred to as *immobile*); 2) vesicles moving in the range of 0.1–0.5 μm/s (*mobile*); and 3) vesicles moving at >0.5 μm/s (*highly mobile*). In control, unstimulated cells, 9% of GLUT4-RFP vesicles were immobile, 66% vesicles were mobile, and 25% were highly mobile (Table 1). Insulin stimulation decreased the percentage of mobile vesicles (from 66 to 46%) and increased the percentage of immobile vesicles (from 9 to 31%). Notably, in Myo1c-depleted cells, insulin stimulation *increased* the proportion of highly mobile GLUT4 vesicles (from 21% in control siNR-treated cells to 40% in Myo1c-depleted cells) and *decreased* the percentage of immobile GLUT4 vesicles (from 31 to 7%; Table 1). As a result, in insulin-stimulated conditions, the average velocity of GLUT4 vesicles was higher in Myo1c-depleted cells (0.48 ± 0.03 μm/s) compared with control cells (0.36 ± 0.03 μm/s, $p < 0.01$). These results indicate that insulin reduces the overall mobility of GLUT4 vesicles, and Myo1c is required for the immobilizing effect of the hormone.

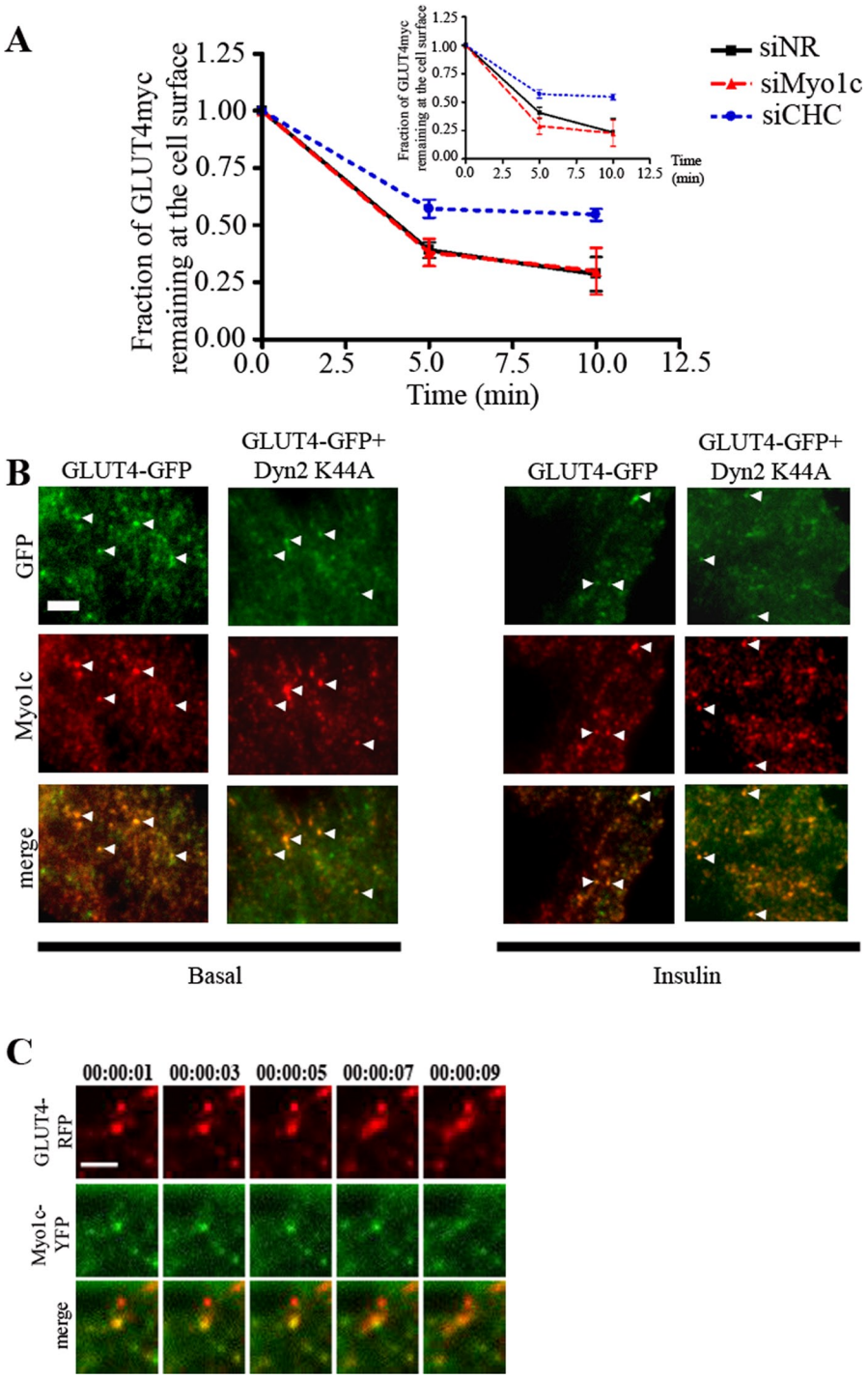

FIGURE 4: Myo1c is not required for GLUT4 internalization and associates with GLUT4 exocytic vesicles. (A) The fraction of GLUT4*myc* remaining at the surface at two times of internalization in L6 myoblasts transfected with siNR, siMyo1c, or siRNA to clathrin heavy chain (CHC). Main panel: insulin-stimulated cells; inset: unstimulated cells. Data are the means ± SE representative of three independent experiments. (B) Endogenous Myo1c (red) colocalizes with GLUT4*myc*-GFP (green) vesicles following inhibition of GLUT4*myc* internalization. L6 myoblasts were transfected with either a 5:1 M ratio of Dyn2 K44A to GLUT4*myc*-GFP or GLUT4*myc*-GFP alone and treated without/with insulin (100 nM, 20 min) at 24 h after transfection; this was followed by immunofluorescence labeling of endogenous Myo1c and imaging by multicolor TIRF microscopy. Arrowheads indicate examples of colocalization. Scale bar: 3 μm. (C) A GLUT4-RFP fusion event is illustrated. WT L6 myoblasts were transiently cotransfected with GLUT4-RFP (red) and Myo1c-YFP (green) and imaged live by multicolor TIRF microscopy (see also Movie S2, a–c). Individual frames shown were captured 2-ms apart. A vesicle containing GLUT4-RFP and Myo1-YFP spreads laterally as it collapses onto the plasma membrane. Scale bars: 2.6 μm.

Myo1c binding to actin immobilizes submembrane GLUT4 and underlies the contribution of the motor protein to GLUT4 translocation

Because Myo1c associated with mobile GLUT4 vesicles near the plasma membrane (Figure 1) and insulin reduced their mobility, we considered the possibility that GLUT4 anchoring into the TIRF zone occurs via the motor protein binding to the submembrane actin cytoskeleton. Accordingly, we explored whether the ability of Myo1c to simultaneously bind actin filaments and membranes is required for insulin-dependent GLUT4 traffic. To this end, we transfected L6-GLUT4*myc* cells with WT-Myo1c-YFP or a truncated mutant, T-Myo1c-YFP, that can bind to membranes via its tail domain but lacks the actin-binding region and is assumed to replace the endogenous Myo1c (as used in Reizes *et al.* [1994]). On its own, overexpression of WT-Myo1c partially elevated surface-exposed GLUT4*myc* (by 1.7 ± 0.17-fold, $p < 0.05$) and caused a further increase in the insulin-stimulated gain (to 5.6 ± 1.1-fold above basal from 3.6 ± 0.8-fold in GFP-expressing control cells; Figure 5A). Conversely, expression of the actin binding–deficient Myo1c-T mutant slightly but significantly lowered basal levels of surface GLUT4*myc* (to 0.7 ± 0.03) and reduced the insulin-dependent net gain (to 2.4 ± 0.6-fold compared with 3.6 ± 0.8-fold in control cells). These results are consistent with previously reported findings in 3T3-L1 adipocytes (Bose *et al.*, 2004) and suggest that Myo1c binding to actin is required for its effect on GLUT4 translocation in both cell types. Given these results, it was necessary to address whether binding of Myo1c to actin is required for vesicular GLUT4/Myo1c colocalization and vesicle dynamic behavior.

WT L6 myoblasts were cotransfected with T-Myo1c-YFP actin binding–deficient mutant and GLUT4-RFP, and their dynamic colocalization was assessed in live cells using TIRF microscopy (Movie S2, a–c). In unstimulated cells, GLUT4-RFP and T-Myo1c-YFP colocalized on both mobile and stationary vesicles (Movie S3, a–c). As in the case of the WT-Myo1c/GLUT4 structures (Figure 1C and Movie S1, a–c), the T-Myo1c/GLUT4–positive vesicular structures displayed short-range movements and long-distance displacements (Movie S2, a–c). Hence the presence of Myo1c on GLUT4 vesicles is independent of the ability of the motor protein to bind to actin. This allowed us to investigate whether the insulin-dependent immobilization of GLUT4 vesicles requires Myo1c binding to actin filaments. L6 myoblasts were cotransfected with GLUT4-RFP and WT-Myo1c-YFP, T-Myo1c-YFP or GFP (control). As discussed above, insulin caused a mild but significant drop in the average velocity of GLUT4-RFP

	<0.1 μm/s Immobile	0.1–0.5 μm/s Mobile	>0.5 μm/s Highly mobile
siNR, basal	9%	66%	25%
siNR, insulin	31%	46%	21%
siMyo1c, basal	16%	51%	28%
siMyo1c, insulin	7%	52%	40%

The velocities of GLUT4-RFP–positive vesicles were determined in cells transfected with fluorescently labeled siNR or siMyo1c. Vesicles in the TIRF zone were classified into three groups based on the velocity of their movement in the TIRF zone: 1) 0 to < 0.1 μm/s (immobile); 2) 0.1–0.5 μm/s (mobile); 3) > 0.5 μm/s (highly mobile). The table lists the percentage (%) that each group represents of the total number of tracked vesicles in the TIRF zone. Two-color TIRF microscopy was used to visualize and image the traffic of GLUT4-RFP in each condition for 15 s before (basal) and 15 s after insulin stimulation (100 nM, 10 min). At least 140 different tracks in six different cells were analyzed for each indicated condition. Individual vesicles were tracked for 15 s or until they disappeared from the TIRF zone.

TABLE 1: Distribution of GLUT4 vesicles in the TIRF zone by their degree of mobility.

vesicular structures in control cells (0.33 μm/s ± 0.05 basal vs. 0.20 μm/s ± 0.04 insulin, $p < 0.05$; Figure 5B). Interestingly, in nonstimulated cells, overexpression of WT-Myo1c-YFP reduced the average velocity of GLUT4 vesicles (from 0.10 ± 0.01 μm/s to 0.33 ± 0.05 μm/s, respectively, $p < 0.05$), and this velocity was further decreased by insulin (to 0.07 ± 0.01 μm/s, $p = 0.05$; Figure 5B). Conversely, the average velocity of GLUT4 vesicles in unstimulated cells expressing T-Myo1c-YFP was significantly higher compared with that in WT-Myo1c-YFP–expressing cells (0.27 ± 0.03 μm/s vs. 0.10 ± 0.01 μm/s, respectively, $p < 0.05$). Most importantly, the average velocity of GLUT4 vesicles in cells overexpressing T-Myo1c-YFP *increased* significantly upon insulin stimulation (from 0.27 ± 0.03 μm/s to 0.40 ± 0.05 μm/s, $p < 0.01$; Figure 5B). These results indicate that insulin reduces the average mobility of GLUT4 vesicles, and Myo1c binding to actin mediates this immobilizing effect. GLUT4 vesicles binding to actin may therefore be the tethering step preceding their docking/fusion with the plasma membrane.

Myo1c knockdown prevents proper actin filament dynamics

The above results suggest that Myo1c links GLUT4 vesicle to actin filaments, and the insulin-dependent reduction in GLUT4 vesicle mobility in the TIRF zone depends on such binding. In addition, Myo1c overexpression on its own can induce cortical actin remodeling in adipocytes (Bose *et al.*, 2004), but it is not known whether the endogenous levels of the motor protein are required for actin dynamics. Insulin causes marked actin polymerization at the cortex of L6 myoblasts (Khayat *et al.*, 2000; Patel *et al.*, 2003; Figure 6A, far left panel), and endogenous Myo1c colocalized with F-actin at sites of membrane ruffles (Figure 6A, marked by arrowheads). In unstimulated cells, Myo1c knockdown significantly reduced the fluorescence intensity of phalloidin-labeled stress fibers (Figure 6B, a, b, and e). Consistent with this finding, these cells displayed a slight reduction (10 ± 0.8%, $p < 0.005$) in cell spreading compared with control cells. Nonetheless, upon insulin stimulation (Figure 6B, c and d), cells with low Myo1c expression did not lose their ability to form actin-rich ruffles, although they experienced a significant loss of cortical actin density in such ruffles (Figure 6Bf) without a significant effect on actin expression (Figure S5). By comparison, there was no change in the organization, integrity, or intensity of microtubules upon Myo1c knockdown (Figure S6). These results support the concept that

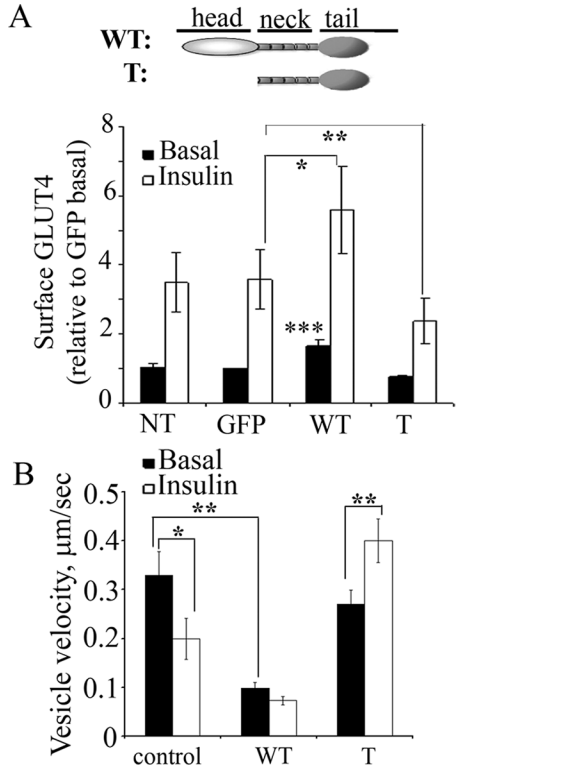

FIGURE 5: Myo1c binding to actin immobilizes submembrane GLUT4 and underlies the contribution of the motor protein to GLUT4 translocation. (A) Cell surface GLUT4*myc* was measured in individual L6-GLUT4*myc* myoblasts transfected with YFP-conjugated Myo1c-WT or Myo1c-T (a mutant unable to bind actin), and the results are presented as fold increases in surface GLUT4*myc* relative to a GFP-transfected basal control (mean ± SE, $n = 3$, *, $p = 0.1$, **, $p = 0.19$, ***, $p < 0.05$). NT, not treated. (B) WT L6 cells were cotransfected with GLUT4-RFP and either GFP (control, $n = 6$), WT-Myo1c-YFP (WT, $n = 4$), or Myo1c-T-YFP (T, $n = 4$). Two-color TIRF microscopy was used to visualize and image the traffic of GLUT4-RFP in each condition for 15 s before and 15 s after insulin stimulation (100 nM, 10min). Data represent the mean vesicle velocity (μm/s) calculated for at least 100 different tracks in each condition acquired by imaging 10–12 time points/s. Individual vesicles were tracked for 15 s or until the vesicle disappeared from the TIRF zone (mean ± SE, *, $p < 0.05$, **, $p < 0.01$).

endogenous Myo1c contributes to actin polymerization independently of insulin stimulation.

Because Myo1c binding to actin is necessary for GLUT4 vesicle immobilization and GLUT4 translocation (Figure 5), we hypothesized that Myo1c facilitates GLUT4 translocation in part by controlling actin polymerization at the membrane cortex. Dynamic actin polymerization depends on the availability of free high-affinity actin filament free barbed ends (FBE). L6 myoblasts transfected with siMyo1c or control siNR were stimulated with insulin and immediately permeabilized just enough to introduce rhodamine-conjugated actin monomers (Koivusalo *et al.*, 2010). The labeled actin readily incorporated into areas of active actin remodeling in both control (87 ± 2% of cells) and Myo1c-knockdown (84 ± 2% of cells) cells (Figure 6C). Control, insulin-stimulated cells formed short and wide FBE-containing ruffles (Figure 6C) that colocalized with phalloidin-decorated F-actin (Figure 6C). The majority of insulin-stimulated cells depleted of Myo1c exhibited lamellipodia-like, contiguous, and thin FBE (42 ± 20% in siMyo1c cells vs. 9.7 ± 4% in siNR cells, $p < 0.05$). Nonetheless, Myo1c knockdown did not inhibit the extent of incorporation

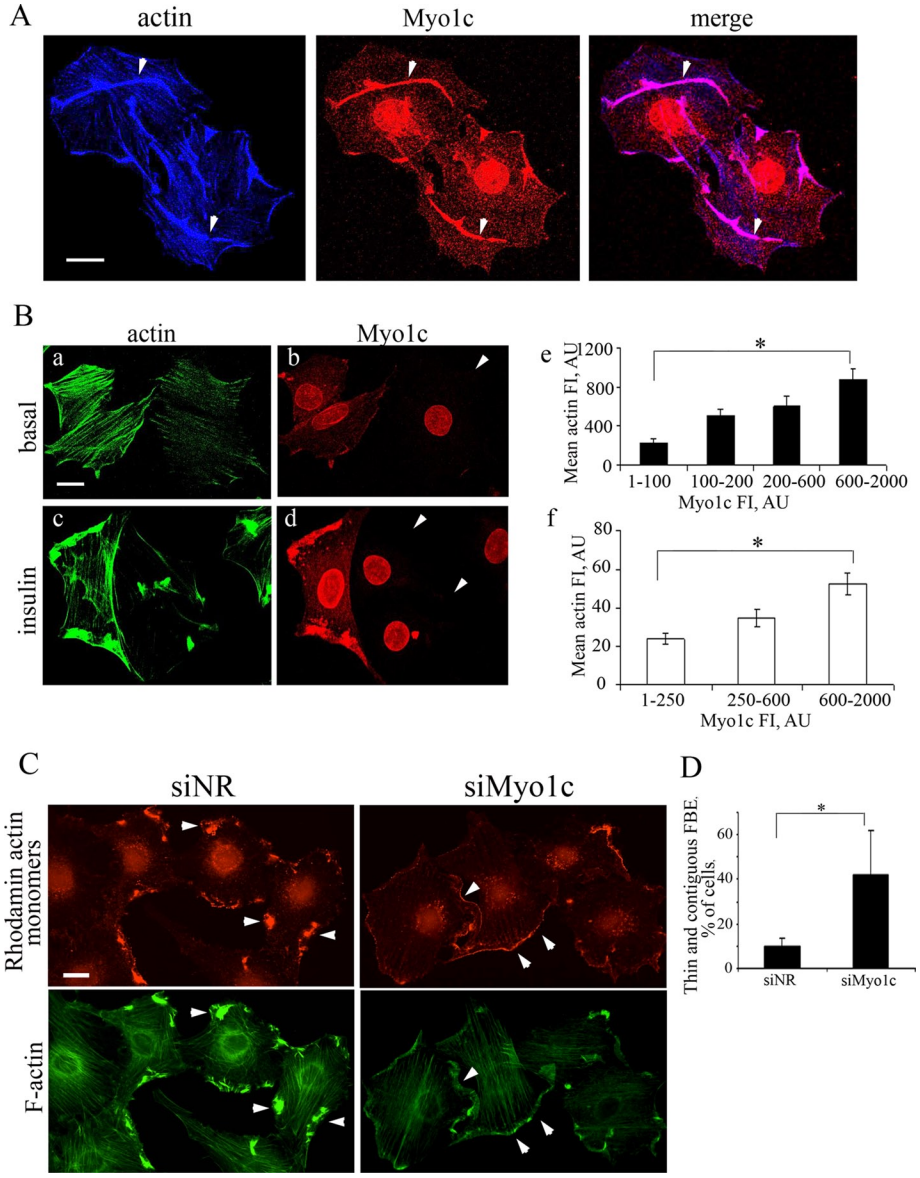

FIGURE 6: Myo1c knockdown prevents proper actin filament reorganization. (A) Myo1c colocalizes with remodeled actin in insulin-induced ruffles. L6-GLUT4*myc* myoblasts were treated with insulin as in Figure 1; this was followed by labeling with phalloidin and Myo1c-specific antibody. Arrowheads mark sites of colocalization. A representative image of three independent experiments is shown. Scale bar: 10 μm. (B, a–d) Filamentous actin is reduced in cells depleted of Myo1c. L6-GLUT4*myc* myoblasts were transfected with siNR or siMyo1c and treated with/without insulin; this was followed by costaining of Myo1c and F-actin. Arrowheads mark cells with efficient Myo1c expression. Representative images of three independent experiments are shown. Scale bar: 10 μm. (B, e and f) Quantification of actin fluorescence intensity as a function of Myo1c expression. The fluorescence intensity of actin and Myo1c in basal (B, e, $n = 82$) or insulin-stimulated (B, f, $n = 78$) control and Myo1c-depleted cells was analyzed using ImageJ. Myo1c (or actin) fluorescence intensities were calculated from images acquired with the same exposure times for control and Myo1c knockdown cells (*, $p < 0.01$). (C) Detection of actin FBEs by imaging of rhodamine-labeled actin monomers (red) in permeabilized siNR- or siMyo1c-treated WT L6 cells after insulin (100 nM, 10 min) stimulation. F-actin was visualized with Alexa Fluor 488–phalloidin (green). Images are representative of three experiments. Note that rhodamine-actin–labeled peripheral structures in Myo1c knockdown cells are thin and long (marked by arrowheads) compared with thick and short ruffles in control cells. Scale bar: 20 μm. (D) Quantification of the percent of cells with thin, elongated FBE ($n = 3$, *, $p < 0.05$).

of rhodamine-actin into FBE compared with cells transfected with siNR (2.1 ± 0.4 vs. 3.4 ± 0.8 fluorescence units, $p = 0.18$). These results suggest that Myo1c does not participate in the insulin-induced generation of FBE (although it may be required for the proper arrangement of the ensuing remodeled actin filaments beneath the plasma membrane).

A connection between Myo1c, CaMKII, and GLUT4 translocation?

A recent study proposed that an insulin-dependent stimulation of CaMKII enhances the ATPase activity of Myo1c in 3T3-L1 adipocytes (Yip *et al.*, 2008). This result was intriguing, since CaMKII is not in the canonical pathway of insulin signals, and its connection to Myo1c was of interest. CaMKII contributes to the stimulation of glucose uptake by insulin in 3T3-L1 adipocytes (Yip *et al.*, 2008) but notably not in skeletal muscle (Yip *et al.*, 2008; Witczak *et al.*, 2010). Surprisingly, the effect of CaMKII on GLUT4 traffic in either muscle or fat cells is unknown. Given the above-described requirement of Myo1c for GLUT4 translocation in muscle cells, and the participation of CaMKII in vesicle fusion events (Kolarow *et al.*, 2007; Ciccone *et al.*, 2008), we explored whether CaMKII is involved in GLUT4 traffic.

As a first step, we examined whether insulin leads to activation of CaMKII in muscle cells. Indeed, stimulation by the hormone led to CaMKII autophosphorylation at T286/7 (Figure S7A), which also induces partially Ca^{2+}-independent "autonomous" CaMKII activity (Coultrap *et al.*, 2010).The contribution of CaMKII to GLUT4 translocation was then assessed by a comprehensive use of pharmacological and molecular inhibitors of CaMKII, dominant-negative mutants of the enzyme, and CaMKII silencing. However, levels of surface GLUT4 were not affected by either: 1) KN-62 (Figure S8A, left panel), which prevents CaMKII stimulation by calmodulin (Tokumitsu *et al.*, 1990); 2) the cell-penetrating inhibitory peptide tat-CN21 (Figure S8A, right panel), which inhibits both stimulated and autonomous CaMKII activity (Vest *et al.*, 2007; Buard *et al.*, 2010); 3) transfection of GFP-fused KIIN (an inhibitory peptide of CaMKII; Figure S8B); 4) the autocamtide-3-derived peptide inhibitor AC3-I (Figure S8B), which inhibits all CaMKII by preventing autophosphorylation (Ishida *et al.*, 1995; Witczak *et al.*, 2010); or 5) the combination of KIIN and AC3-I (Figure S8B). Of note, KN-62, but not CN21, reduced both basal and insulin-stimulated glucose uptake (Figure S7B), perhaps as a result of interactions with the glucose-binding site on GLUT4 itself.

As a complement to these experiments using small-molecule or peptide inhibitors, L6-GLUT4*myc* cells were transiently transfected with wild-type or mutant versions of CaMKIIβ. Neither WT-GFP-CaMKIIβ, its ATP binding–impaired K43R mutant,

or a constitutively active T287D mutant affected surface GLUT4*myc* relative to GFP-expressing control cells (Figure S8C). However, it remained possible that other isoforms of the enzyme might be involved, since L6 myoblasts express the CaMKII α, β, γ, and δ isoforms (Figure S9). Therefore we resorted to silencing the expression of the most abundant one, CaMKIIδ. Using siRNA oligonucleotides to this isoform, we achieved a 76 ± 5% loss in total CaMKII (Figure S8D) and a significant reduction in the phospho-CaMKII signal detected by immunofluorescence. However, there was no concomitant drop in insulin-induced GLUT4 translocation under these conditions (Figure S8E).

Thus, while insulin activated CaMKII, an exhaustive test of strategies did not find any requirement for this activity in GLUT4 translocation in response to insulin. Therefore it is unlikely that CaMKII is involved in the Myo1c-dependent mobilization of the transporter to the surface of muscle cells.

DISCUSSION

Myo1c is a membrane-bound, actin-based motor protein that mediates membrane–cytoskeletal interactions and has been implicated in diverse phenomena involving vesicle traffic including exocytosis, endocytosis, cell migration, and in the generation of plasma membrane tension (Barylko *et al.*, 2005; McConnell and Tyska, 2010). Recent studies show that silencing Myo1c expression partly reduces insulin-mediated glucose uptake into skeletal muscle (Witczak *et al.*, 2010) and lowers GLUT4 translocation in 3T3-L1 adipocytes (Bose *et al.*, 2002, 2004; Yip *et al.*, 2008). In this study, we provide evidence for the molecular mechanism underpinning this response. This was shown in skeletal muscle cells, given the prominence of skeletal muscle in the physiological uptake of glucose from the blood.

We first show that Myo1c is not present in the perinuclear region, where the majority of GLUT4 is located in resting cells. However, the two proteins colocalize in peripheral areas of the cell. Within the 200-nm reach of the inner surface of the plasma membrane (the TIRF zone), Myo1c and GLUT4 colocalize on vesicular structures in both L6 myoblasts and isolated single fibers of FDB muscle. Based on their velocity, these GLUT4/Myo1c vesicles distribute into three classes. Insulin increased the proportion of immobile vesicles within the TIRF zone, and effectively reduced the GLUT4 vesicles' average velocity. This behavior was lost upon Myo1c depletion, causing an increase in the average vesicular velocity, which concomitantly prevented exposure of GLUT4 at the outer face of the membrane. Moreover, Myo1c depletion reduced the amount of GLUT4 vesicles at the TIRF zone, but not their spreading from perinuclear to cytosolic distribution, suggesting that Myo1c-dependent immobilization retains GLUT4 vesicles beneath the membrane. Indeed, overexpressing Myo1c decreased the average mobility of GLUT4 vesicles in the TIRF zone, concomitant with potentiation of insulin action on GLUT4 translocation. These effects were lost when a mutant Myo1c unable to bind actin filaments, rather than WT Myo1c, was transfected. We propose that Myo1c helps tether GLUT4 vesicles to submembrane actin filaments, thereby reducing their mobility, as a preamble to GLUT4 vesicle docking and fusion with the plasma membrane to enact increased glucose uptake.

Characteristics of GLUT4 vesicle dynamics and effect of insulin

GLUT4 vesicles in the TIRF zone could be segregated into three groups, depending on whether they have negligible, medium, or high velocity. The proportion of these pools of vesicles was 9, 66, and 25% in resting cells, respectively. Insulin increased the proportion of immobile vesicles, changing the distribution to 31, 46, and 23%, and, consistently, decreased the overall vesicular average velocity (from 0.33 µm/s ± 0.05 to 0.20 µm/s ± 0.04). Insulin stimulation also reduced the number of GLUT4 vesicles in the TIRF zone, presumably because they are consumed by fusion with the plasma membrane faster than they arrive at this zone. These findings are consistent with change in the speed and number of GLUT4 puncta in isolated FDB muscle fibers in response to insulin (Lizunov *et al.*, 2012).

Further, we demonstrate for the first time that Myo1c and GLUT4 move on the same puncta in the TIRF zone (Figure 1 and Movie S1, a–c). This suggests that Myo1c participates in GLUT4 traffic events in this zone. Accordingly, Myo1c depletion promoted GLUT4 vesicle mobility, elevating the proportion of highly mobile vesicles from 21% in the corresponding control cells to 40%. This resulted in an increase in the average vesicular velocity from 0.36 ± 0.03 µm/s to 0.48 ± 0.03 µm/s. We speculate that such a rise in vesicle mobility may result from loss of binding of vesicular Myo1c to actin filaments.

Notably, the range in GLUT4 vesicle speeds in myoblasts was similar to that of mobile GLUT4 vesicles in isolated FDB muscle fibers from transgenic mice with muscle-specific expression of hemagglutinin (HA)-GLUT4-GFP (Lizunov *et al.*, 2012). In both systems, the vesicle velocity was heterogeneous and ranged from 0.1 to 2 µm/s with no apparent preferential directionality (Lizunov *et al.*, 2012; Table 1). In contrast to our findings, however, Lizunov *et al.* (2012) found that most of the HA-GLUT4-GFP structures were stationary, with only 10% exhibiting displacements exceeding 1 µm (their limit of detection). That limit may have missed the vibrational movements that we detected in myoblasts (detection limit of 0.1 µm). Differences may also arise from the complexity of mature muscle fibers relative to myoblasts, as the space and vesicular movement in the former may be restricted by the abundance of contractile fibers.

It is important to note that the number of GLUT4 vesicles in the TIRF zone decreased in unstimulated cells depleted of Myo1c, possibly as a result of diminished tethering. Hence Myo1c determines GLUT4 vesicle mobility, even in the absence of insulin. This effect is exacerbated in the insulin-stimulated state, in which Myo1c depletion precludes the insulin-dependent drop in vesicle number and mobility exerted by the hormone. We speculate that, in Myo1c-containing cells, the insulin-induced polymerization and remodeling of actin filaments beneath the plasma membrane increases the probability of vesicle immobilization. This possibility is supported by the observation that a Myo1c mutant unable to bind actin filaments still bound to GLUT4 vesicles but prevented the insulin-dependent reduction in vesicle mobility and concomitantly abated GLUT4 insertion in the membrane (Figure 5).

Effect of Myo1c on actin dynamics

Myo1c overexpression causes actin polymerization in adipose cells by association with Rictor (Hagan *et al.*, 2008), but the mechanism and implication of this phenomenon remains obscure. Because overexpression might induce a nonphysiological response, we tested whether, conversely, Myo1c depletion would prevent actin polymerization (documented by measuring actin monomer incorporation into filament FBE). Whereas the net amount of actin incorporation into FBE was not altered by Myo1c depletion, Myo1c-depleted cells showed thinner insulin-induced lamellipodia-like ruffles that run extensively along the cell periphery, compared with the short and dense ruffles observed in insulin-stimulated control cells. We surmise that Myo1c knockdown precludes proper localization of

FBE and that normally Myo1c directs actin monomer incorporation to specific loci beneath the plasma membrane. Myo1c knockdown also reduced the net amount of polymerized actin. The molecular mechanism by which Myo1c controls actin dynamics is not known, but it may be mediated via Arp2/3 binding, as is the case for the fungal Myo1 orthologues (Evangelista *et al.*, 2000; Lechler *et al.*, 2000), or Myo1c may compete with the binding of F-actin–severing proteins (e.g., cofilin), preventing proper actin dynamics, among other possibilities.

Interestingly, Myo1c knockdown also reduced the intensity of stress fibers in unstimulated cells. Because there was a decrease in the number of vesicles in the TIRF zone under these conditions, yet surface levels of GLUT4 were not altered in the absence of insulin treatment, stress fibers may contribute to providing GLUT4 vesicles to the vicinity of the plasma membrane in the basal state (as seen in Figure 1). Whether stress fiber integrity/formation would allow GLUT4 mobility toward the cell periphery requires future investigation.

Steps in GLUT4 traffic controlled by Myo1c

The perinuclear-to-cytosolic dispersion of GLUT4 induced by insulin was preserved in Myo1c knockdown cells. This is consistent with this step being mediated by microtubule- but not actin-based movement, in analogy with other systems (Nascimento *et al.*, 2003). In contrast, in Myo1c knockdown cells, the net amount of GLUT4 vesicles in the TIRF zone was reduced, suggesting GLUT4 vesicles arriving at this zone cannot be retained by the normal mechanisms.

Most models of GLUT4 traffic propose that vesicles reaching the plasma membrane emanate from "storage" or "primed" pools (Blot and McGraw, 2008; Brewer *et al.*, 2011) and suggest a tethering step from whence docking and fusion proceed. However, the role of tethering in this progression is unknown. While we propose that Myo1c tethers GLUT4 vesicles to actin filaments, we can only speculate on the consequence of this step. Tethered/immobilized vesicles may have more opportunity for efficient interaction with membrane proteins, allowing the participating vesicular VAMP2 to effectively engage with syntaxin4 and SNAP23 on the plasma membrane (SNARE proteins have been shown to mediate fusion of insulin-sensitive GLUT4 vesicles with the membrane [Foster and Klip, 2000; Williams and Pessin, 2008]). The presence of Myo1c in ruffled regions might also indicate a Myo1c association with the plasma membrane, potentially through inositol phospholipids (Hokanson *et al.*, 2006) or plasma membrane–associated proteins (Chen *et al.*, 2007). Whether Myo1c also regulates docking and fusion with the plasma membrane requires further investigation.

Insulin regulates the Myo1c ATPase activity in 3T3-L1 adipocytes (Bose *et al.*, 2004) and causes Myo1c phosphorylation at a site that binds calmodulin light chains (Yip *et al.*, 2008). This suggested that phosphorylation mediated by CaMKII would activate Myo1c and, consistent with this prediction, inhibition of the kinase reduced insulin-stimulated glucose uptake in adipocytes (Yip *et al.*, 2008), although GLUT4 translocation was not assessed. These observations were intriguing and prompted us to probe the potential role for CaMKII in insulin-stimulated GLUT4 traffic in muscle cells. Interestingly, insulin promoted CaMKII phosphorylation at the autoregulatory site of the kinase that would relieve autoinhibition (Bayer *et al.*, 2001, 2006; Figure S7A). CaMKII also colocalized and coimmunoprecipitated with α-actinin-4 (Supplementary Figure S7, C and D), a protein we had previously shown to interact with GLUT4 and actin and to be required for normal GLUT4 traffic to the plasma membrane (Foster *et al.*, 2006; Talior-Volodarsky *et al.*, 2008). We had hypothesized that CaMKII—possibly acting through α-actinin-4—might be required for insulin-dependent GLUT4 translocation. However, this link did not materialize, as an exhaustive strategy to inhibit the CaMKII or deplete its expression was inconsequential to GLUT4 translocation (Figure S8), which nonetheless required Myo1c.

In conclusion, we present evidence that insulin reduces the mobility of GLUT4 vesicles within the TIRF zone, and Myo1c is required for such immobilization through its association with submembrane actin. Concomitantly, delivery of GLUT4 for docking/fusion may be facilitated by the Myo1c-enhanced polymerization of actin filaments in this region. In this manner, Myo1c contributes to insulin-dependent GLUT4 exposure at the surface of muscle cells.

MATERIALS AND METHODS

Reagents, siRNA, and constructs

Monoclonal anti-*myc* antibody and monoclonal anti-CaMKII were from Santa Cruz Biotechnology (Santa Cruz, CA). Polyclonal anti–phosphorylated Akt (Ser473), anti-Akt, ERK1/2 antibodies were from Cell Signaling Technology (Beverly, MA). Fluorescein isothiocyanate (FITC) conjugate of monoclonal anti-tubulin (clone DMIA) and polyclonal anti-Myo1c were from Abcam (Cambridge, MA). Polyclonal anti–phosphorylated Thr286/7-CaMKII was from Phosphosolutions (Aurora, CO). Rabbit polyclonal anti–α-actinin-4 antibody was from Alexis Biochemicals (San Diego, CA). Anti-AS160 and anti–phosphorylated (Thr642) AS160 were from Millipore (Billerica, MA). Anti–γ-actin, anti–α-SMA (smooth muscle actin), and anti–β-actin antibodies were kindly provided by Boris Hinz (University of Toronto, Toronto, ON). Monoclonal anti-HA antibody (clone HA.11) was from Covance (Berkeley, CA). Alexa Fluor 488–ConA conjugate, Alexa Fluor 633–phalloidin, and Alexa Fluor 488–phalloidin were purchased from Molecular Probes (Eugene, OR). Human insulin was purchased from Eli Lilly (Indianapolis, IN). Collagenase IV was from Worthington Biochemical Corporation (Lakewood, NJ). Phenol-red free BD Matrigel Matrix was from BD Biosciences (Bedford, MA). YFP-tagged YFP-Myo1c and YFP-Myo1c (T) plasmids were kindly provided by Michael P. Czech (University of Massachusetts Medical School, Worcester, MA). Expression vectors containing GFP conjugated to the CaMKII inhibitory AC3-I (KKALHRQEAVDCL) or the CaMKII control AC3-C (KKALHAQERVDCL) peptides were kindly provided by Mark E. Anderson (University of Iowa, Iowa City, IA). A plasmid coding for the CaMKII inhibitory peptide KIIN (KRPPKLGQIGRAKRVVIEDDRIDDVLK) (Chang *et al.*, 2001) fused to GFP (GFP-KIIN) was obtained from T. R. Soderling (Oregon Health and Sciences University, Portland, OR). Plasmids, encoding GFP-CaMKIIβ wild-type and its GFP-tagged mutants A303R (CaM-binding impaired), K43R (ATP-binding impaired), and T287D (constitutively active), as well the CaMKII inhibitor peptide tat-CN21 (tatCN21) and the scrambled sequence control (tatCtrl), were as previously described (Vest *et al.*, 2007). Dynamin-2 K44A cDNA was a kind gift from Mark McNiven (Mayo Clinic, Rochester, NY). GLUT4-RFP was generated by amplification of GLUT4*myc* fragment from GLUT-4*myc*-GFP (Ueyama *et al.*, 1999) and subcloning into pmCherry-N1 (Clontech, Mountain View, CA) using *Eco*RI/*Age*I restriction sites. VAMP2-HA was generated by amplification of VAMP2 fragment from VAMP2-GFP (Randhawa *et al.*, 2008) and subcloning into pQCXIH using *Age*I-*Pac*I restriction sites. siRNAs targeted against Myo1c (5′-atcatgtgatcgagacactaa-3′), and (5′-cacggctgaattctcggtgat-3′), MyoIIA (5′-aaggatgtggatcgaatcatt-3′), clathrin heavy chain-1 (5′-aac ccg agt tat gga gta tat-3′) (Antonescu *et al.*, 2008), and nonrelated control (5′-aataaggctatgaagagatac-3′) were purchased from Qiagen (Chatsworth, CA) and named siMyo1c, siMyoIIA, and siNR. ON-TARGETplus SMARTpool siRNA targeted against CaMKIIδ were

obtained from Dharmacon (CaMKIIδ; accession number L-099520, #1, 5′- gtaaatcauugtcacctaa-3′; #2, 5′-gatgggaagtggcagaata-3′; #3, 5′-gtagactgcttgaagaaat-3′; #4, 5′-cacagtacauggatggaaa-3′; Lafayette, CO).

Cell culture and transfection

Rat L6 myoblasts without (WT L6) or with stable expression of *myc*-tagged GLUT4 L6-GLUT4*myc*) were cultured as described previously (Ueyama *et al.*, 1999). To create L6-GLUT4*myc* myoblasts stably expressing human AS160 (cDNA a kind gift from G. E. Lienhard, Dartmouth Medical School) or VAMP2-HA, we cloned the cDNAs into pQXIP or pQCXIH retroviral vectors (BD Biosciences), respectively. Retroviral supernatants were produced in Phoenix packaging cells obtained from G. P. Nolan (Stanford University, Stanford, CA) according to their protocol (www.stanford.edu/group/nolan/index.html) and used to infect L6-GLUT4*myc* myoblasts. Forty-eight hours postinfection, the cultures were treated with 2 µg/ml puromycin (for L6-GLUT4*myc*-AS160) or 200 µg/ml hygromycin (for L6-GLUT4*myc*-VAMP2-HA) for 7 d to create a stable pool of clones (L6-GLUT4*myc*-AS160) that were cultured in the same manner as L6-GLUT4*myc* cells. Transfection of siRNAs or cDNA plasmid constructs was performed with Lipofectamine RNAiMAX or Lipofectamine 2000, respectively, as per the manufacturer's instructions (Invitrogen, Carlsbad, CA). Transfection of siRNA proceeded for 24 h and of cDNA for 4–6 h; cells were then allowed to recover or were trypsin-treated and transferred to glass coverslips 24–48 h before experimentation.

GLUT4myc immunoprecipitation and immunoblotting

L6-GLUT4*myc* myoblasts seeded in 10-cm dishes were grown to confluence and serum-deprived for 3 h before stimulation with 100 nM insulin for 20 min. Lysates (1.5 mg protein) were immunoprecipitated with 40 µl of 9E10 Monoclonal Affinity Matrix as previously described (Foster *et al.*, 2006). Cells were washed quickly with cold phosphate-buffered saline (PBS), and lysed in 1× Laemmli sample buffer supplemented with a cocktail of protease and phosphatase inhibitors (NaF 1 mM and $NaOV_3$ 1 mM). Samples were resolved by 10% SDS–PAGE and subjected to immunoblotting.

Glucose uptake, GLUT4 translocation, and GLUT4 internalization in cell monolayers

L6-GLUT4*myc* cells grown in 24-well plates and serum-starved for 3–5 h were treated as indicated in the figure legends and incubated with or without 100 nM insulin for 20 min; uptake of 2-deoxy-[^{3}H] glucose was then measured as previously described (Tamrakar *et al.*, 2011). Nonspecific uptake was determined in the presence of cytochalasin B (20 µM) and subtracted from all values. GLUT4*myc* internalization was measured as described earlier (Antonescu *et al.*, 2008). Surface GLUT4myc levels were determined in paraformaldehyde-fixed, nonpermeabilized L6-GLUT4myc myoblast monolayers (grown in 24-well plates) labeled with anti-*myc* antibody, which was followed by HRP-conjugated secondary antibody, as previously described (Ueyama *et al.*, 1999; Tamrakar *et al.*, 2011).

Transferrin recycling assay

L6-GLUT4*myc* cells were serum-starved for 2 h and then incubated with 50 µg/ml of A555-conjugated transferrin (Invitrogen) in serum-free medium supplemented with 1% bovine serum albumin (BSA), without or with insulin (100 nM) for 10 min at 37°C. One plate of cells was placed on ice; washed twice with PBS, twice with acid buffer (0.15 M NaCl, 0.1 M glycine, pH 3.0), twice with PBS; and fixed with 4% paraformaldehyde (PFA) for 1 h at room temperature. A second plate was chased with 500 µg/ml holo-transferrin (Sigma-Aldrich, St. Louis, MO) for 10 min at 37°C with or without insulin, washed, and fixed as above. All cells were quenched with 0.1 M glycine for 10 min, washed once with PBS, and processed for fluorescence detection of A555-conjugated transferrin in single cells.

Fluorescence microscopy and cell-surface GLUT4myc detection in single cells

Immunofluorescence detection of surface GLUT4*myc* in L6-GLUT4*myc* myoblasts was performed as previously described (Torok *et al.*, 2004). After 3-h serum starvation, cells were stimulated without and with insulin (100 nM) for 10 min at 37°C. Cells were quickly washed twice with cold PBS, fixed with 3% (vol/vol) PFA, and blocked with 5% (vol/vol) milk. Surface GLUT4*myc* was stained with anti-*myc* primary antibody, which was followed by secondary antibody. For surface GLUT4*myc* detection in single cells, WT L6 cells were transiently transfected with GLUT4-RFP or GLUT4*myc*-GFP, fixed as above but not permeabilized, and incubated with monoclonal anti-*myc* antibody and Cy5-conjugated secondary antibody. GLUT4 translocation was calculated as the ratio of Cy5 to total RFP or GFP fluorescence intensity per cell, in 20 cells per condition. For detecting surface GLUT4*myc* and intracellular Myo1c or CaMKII, surface GLUT4*myc* was first labeled as above; this was followed by membrane permeabilization with 0.5% Triton X-100 for 3 min, for subsequent Myo1c or pThr286/7 CaMKII immunolabeling. For double Myo1c and F-actin or pThr286/7 CaMKII labeling, cells were fixed with 3% PFA in PBS for 10 min on ice and an additional 10 min at room temperature, then permeabilized with 0.5% Triton X-100 for 3 min and stained with Alexa Fluor 488–phalloidin, anti-Myo1c antibody, or anti-pThr286/7CaMKII antibody, as indicated. For ConA labeling of the cell surface, cells were fixed with 3% PFA for 20 min, incubated with ConA (50 µg/ml PBS) at 4°C for 30 min, and fixed with 3% PFA for 20 min at room temperature. Cells were then permeabilized with 0.5% Triton X-100 for 3 min and stained with an anti-Myo1c antibody. For double tubulin/Myo1c staining, cells were fixed for 10 min in cold (–20°C) methanol and then labeled with FITC-conjugated anti-tubulin and anti-Myo1c antibodies. Fluorescence images were acquired on a Zeiss LSM 510 META laser-scanning confocal microscope (Thornwood, NY), using a 60×/1.4 numerical aperture (NA) Plan-Apochromat objective and Zeiss AIM software. Whole cells were scanned along the *z*-axis and a single composite image (collapsed *xy* projection) of the optical cuts per cell was generated using LSM5 Image software. Images were converted into TIFF files by ImageJ version 1.42 (National Institutes of Health [NIH], http://rsb.info.nih.gov/ij) software and arranged into figures using Adobe Photoshop (San Jose, CA).

Image analysis

Images were analyzed using ImageJ to quantify fluorescence intensities from unmanipulated raw images. For Figures S1C and S6B, ROIs on the plasma membrane (ruffles), inside the cell (cytosol), or the entire cell plus an area outside the cell (background) were manually traced, and their mean fluorescence intensities were quantified after background subtraction. Vesicle number at the TIRF zone in fixed cells was analyzed using the Find 2D spots function of the Velocity 5.5 package (Improvision, Lexington, MA) and applied to the polygon drawn around the cell. Before analysis, images were adjusted for better vesicle segmentation, and the vesicle number in the evanescent field was normalized to total GLUT4*myc*-GFP epifluorescence (vesicle number in TIRF zone/GLUT4-GFP epifluorescence ratio). For colocalization analysis, TIRF images were acquired at high magnification (150×/1.45 NA objective), and ROIs

containing vesicular GLUT4*myc*-GFP were cropped from the entire image. The degree of colocalization was quantified by Pearson's coefficient of correlation (*R*) using the Volocity colocalization measurement tool and subjected to Student's *t* test statistical analysis. The manual track function of the Velocity 6.1 package was used to analyze GLUT4 vesicle velocity and displacement at the TIRF zone. Single GLUT4 puncta were marked as follows: the particle center was manually located and traced for the indicated time intervals or until its disappearance from the TIRF zone. Data are presented as means ± SEM. Statistical significance was analyzed using Student's *t* test.

For cell spreading quantification, L6 myoblasts were fixed, the actin cytoskeleton was labeled with phalloidin, and images of mock and Myo1c-depleted cells were captured by confocal fluorescence microscopy, which was followed by image deconvolution. The mean cellular area of cells was measured with Velocity 5.5.

Video microscopy

For studying the colocalization between GLUT4-RFP and WT-Myo1c-YFP or T-Myo1c-YFP (Movies S1 and S2 and Figure 1C) in multicolor TIRF microscopy, WT L6 cells on 18-mm #1.5 round glass coverslips (Zeiss) were transfected and analyzed 24 h after transfection. Thirty minutes before observations, the medium was switched to HEPES-containing RPMI-1640. Images were acquired on an Olympus IX81 microscope equipped with a dual-laser (488 nm, 561 nm) CellTIRF temperature control unit using the 150×/1.45 NA objective and a QuantEM back-thinned EM-CCD. The penetration of the evanescent field was measured to be 110 nm. Images were acquired using MetaMorph and CellCut acquisition software and converted into TIFF files by ImageJ software (NIH). Images were filtered using the Unsharp Mask plug-in of Image J and converted to movies.

For study of GLUT4-RFP vesicle dynamic behavior, WT L6 myoblasts were transfected with the listed siRNA oligonucleotides, replated on 18-mm #1.5 round glass coverslips (Zeiss), cultured for 24 h, and then transfected with indicated cDNA constructs (GLUT4-RFP/WT-Myo1c-YFP/T-Myo1c-YFP) for an additional 24 h. Cells were serum-starved for at least 3 h, the culture medium was switched to HEPES-containing RPMI-1640, and the cells were imaged on a Olympus IX81 microscope equipped with a dual-laser CellTIRF unit, as above, using Volocity 4.3.2 build 23 and CellCut acquisition software. Individual cells were imaged in the basal state for the indicated time intervals, the acquisition was stopped, and insulin was added for 10 min (final concentration 100 nM). Imaging of the same cells continued for indicated time intervals.

Actin-free barbed-end assay

Filament barbed end (FBE) were determined by a modification of previously described methods (Chan *et al.*, 1998; Frantz *et al.*, 2008; Koivusalo *et al.*, 2010). Briefly, serum-starved myoblasts on coverslips were incubated without or with insulin (100 nM) for 20 min. Cells were permeabilized for 15 s in 20 mM HEPES, 140 mM NaCl, 3 mM KCl, 2 mM $MgCl_2$, 2 mM EGTA, 5 mM glucose, 1% BSA, and 0.5 mM ATP (pH 7.5) containing 0.04% saponin and 0.02 μg/μl rhodamine-labeled rabbit skeletal muscle actin. After 15 s, the solution was diluted threefold with permeabilization buffer without saponin and rhodamine-actin, and incubation continued for 3 min, followed by fixation in 3% PFA (20 min). For comparison of actin FBE formation in control and Myo1c knockdown cells, the area encompassing each single, continuous, rhodamine-labeled ruffle was manually traced on highly magnified images using the freehand tool, the ruffle mean fluorescence intensities were measured, and background subtraction using confocal fluorescence microscopy was done. The fluorescence intensity is reported as the ratio of the fluorescence of the ruffle relative to that of the cytosol. Images illustrated were acquired by epifluorescence.

Detection of CaMKII isoforms and Myo1c expressed in L6 cells by reverse transcriptase PCR (RT-PCR)

Excision of rat muscle was approved by the Animal Care Committee of the Hospital for Sick Children. Total RNA (200 ng) from rat skeletal muscle, L6-GLUT4myc myoblasts, and myotubes was prepared using guanidine isothiocyanate-phenol-chloroform and used for one-step RT-PCR, according to the manufacturer's instructions (Qiagen, Valencia, CA). Primers were designed using Primer3 software [CaMKIIα: forward (FWD) 5′-ctgaaccctcacatccacct-3′ and reverse (REV), 5′-acgatctgccattttccatc-3′]; [CaMKIIβ: FWD, 5′-gaaagcagacg-gagtcaagc-3′ and REV, 5′-gttggtgctgtcggaagatt-3′], [CaMKIIγ: FWD, 5′-gcgtcaagaaaaggaagtcg3′ and REV, 5′-ctggctcaaaggaagtgagg-3′], [CaMKIIδ: FWD, 5′-ctggcacacctgggtatctt-3′ and REV, 5′- cactgtgtc-ccattctggtg-3′], [Myo1c: FWD, 5′-cctggtggaggagaaattca-3′ and REV, 5′- gtgtcctccagcttctccag-3′] and [GAPDH as a control FWD, 5′-tgccactcagaagacgtggg-3′ and REV, 5′-ttcagctctgggatgacctt-3′] and used in the following PCR program on Thermal Cycler (Bio-Rad, Hercules, CA): RT at 50°C/30 min, denaturation at 95°C/15 min and repeated cycles of denaturation at 94°C/45 s, annealing at 57°C/45 s, and extension at 72°C/45 s, followed by final extension at 72°C/10 min. After RT, CaMKII α, β, γ, or δ and GAPDH were amplified for 35 (CaMKII α, β, γ, δ) and 29 (GAPDH) cycles, after titration for each gene-specific primer pair to ensure linearity.

Analysis of isolated muscle fibers from adult mice

All animal-use protocols were approved by the Hospital for Sick Children's Animal Care Committee in accordance with the Canadian Council of Animal Care guidelines. WT-Myo1c-YFP and/or GLUT4-RFP plasmids (total ~20 μg, at 1 μg/μl) were injected subcutaneously into the FDB muscle of male mice (12 wk old); this was followed by electroporation as previously described (DiFranco *et al.*, 2009). Twenty 20-ms pulses of 100 V with 980-ms intervals were delivered using a CUY21 EDIT square electroporator (TR-Tech, Tokyo, Japan). Mice were killed 10 d later, and FDB muscles were obtained by enzymatic digestion of the whole muscle with type IV collagenase (600 U/ml, 90 min), followed by mechanical dissociation with fire-polished Pasteur pipettes. Isolated FDB fibers were plated on Matrigel-coated coverslips (diluted 1:4 in serum-free DMEM). After 2.5 h, fibers were washed gently with PBS and fixed with 4% PFA/PBS for 20 min at room temperature, washed again in PBS, and quenched with 0.125 M glycine (10 min). Fibers cotransfected with YFP-Myo1c and GLUT4-RFP were visualized under a two-color TIRF microscope, as described above. For visualization of GLUT4-RFP with endogenous Myo1c, isolated muscle fibers were fixed as above, permeabilized with Triton 0.1%/PBS (15 min), quenched with 0.125 M glycine (10 min), blocked with BSA3%/PBS (10 min), and incubated overnight at 4°C with anti-Myo1c, which was followed by Alexa Fluor 488–conjugated secondary antibody (1 h) at room temperature. After being washed with PBS, fibers were visualized by epifluorescence microscopy.

ACKNOWLEDGMENTS

This work was supported by grant MT12601 to A.K. from the Canadian Institutes of Health Research (CIHR). S.B. was supported by fellowship from the Canadian Diabetes Association and the Banting and Best Diabetes Center. T.C. was supported by a Banting Scholarship from CIHR. C.O.-F. was supported by visiting doctoral scholarship UCH0713 from MECESUP. We thank Zhi Liu for technical assistance in this study; Shuhei Ishikura for

generating the pQCXIH retroviral vector encoding VAMP2-HA; Michael P. Czech, Mark E. Anderson, Thomas R. Soderling, and Boris Hinz for generous supplies of constructs or antibodies; Michael Woodside and Paul Paroutis for help with confocal and TIRF microscopy; and François Aguet for generously providing access to the computer algorithms used to calculate properties of vesicles in the TIRF zone.

REFERENCES

Adams RJ, Pollard TD (1989). Binding of myosin I to membrane lipids. Nature 340, 565–568.

Antonescu CN, Diaz M, Femia G, Planas JV, Klip A (2008). Clathrin-dependent and independent endocytosis of glucose transporter 4 (GLUT4) in myoblasts: regulation by mitochondrial uncoupling. Traffic 9, 1173–1190.

Barylko B, Jung G, Albanesi JP (2005). Structure, function, and regulation of myosin 1C. Acta Biochim Pol 52, 373–380.

Bayer KU, De Koninck P, Leonard AS, Hell JW, Schulman H (2001). Interaction with the NMDA receptor locks CaMKII in an active conformation. Nature 411, 801–805.

Bayer KU, LeBel E, McDonald GL, O'Leary H, Schulman H, De Koninck P (2006). Transition from reversible to persistent binding of CaMKII to postsynaptic sites and NR2B. J Neurosci 26, 1164–1174.

Blanchoin L, Pollard TD, Mullins RD (2000). Interactions of ADF/cofilin, Arp2/3 complex, capping protein and profilin in remodeling of branched actin filament networks. Curr Biol 10, 1273–1282.

Blot V, McGraw TE (2008). Molecular mechanisms controlling GLUT4 intracellular retention. Mol Biol Cell 19, 3477–3487.

Bogan JS, Kandror KV (2010). Biogenesis and regulation of insulin-responsive vesicles containing GLUT4. Curr Opin Cell Biol 22, 506–512.

Bose A, Guilherme A, Robida SI, Nicoloro SM, Zhou QL, Jiang ZY, Pomerleau DP, Czech MP (2002). Glucose transporter recycling in response to insulin is facilitated by myosin Myo1c. Nature 420, 821–824.

Bose A, Robida S, Furcinitti PS, Chawla A, Fogarty K, Corvera S, Czech MP (2004). Unconventional myosin Myo1c promotes membrane fusion in a regulated exocytic pathway. Mol Cell Biol 24, 5447–5458.

Brewer PD, Romenskaia I, Kanow MA, Mastick CC (2011). Loss of AS160 Akt substrate causes Glut4 protein to accumulate in compartments that are primed for fusion in basal adipocytes. J Biol Chem 286, 26287–26297.

Brozinick JTJr., Hawkins ED, Strawbridge AB, Elmendorf JS (2004). Disruption of cortical actin in skeletal muscle demonstrates an essential role of the cytoskeleton in glucose transporter 4 translocation in insulin-sensitive tissues. J Biol Chem 279, 40699–40706.

Buard I, Coultrap SJ, Freund RK, Lee YS, Dell'Acqua ML, Silva AJ, Bayer KU (2010). CaMKII "autonomy" is required for initiating but not for maintaining neuronal long-term information storage. J Neurosci 30, 8214–8220.

Cao H, Thompson HM, Krueger EW, McNiven MA (2000). Disruption of Golgi structure and function in mammalian cells expressing a mutant dynamin. J Cell Sci 113, 1993–2002.

Chan AY, Raft S, Bailly M, Wyckoff JB, Segall JE, Condeelis JS (1998). EGF stimulates an increase in actin nucleation and filament number at the leading edge of the lamellipod in mammary adenocarcinoma cells. J Cell Sci 111, 199–211.

Chang BH, Mukherji S, Soderling TR (2001). Calcium/calmodulin-dependent protein kinase II inhibitor protein: localization of isoforms in rat brain. Neuroscience 102, 767–777.

Chen XW, Leto D, Chiang SH, Wang Q, Saltiel AR (2007). Activation of RalA is required for insulin-stimulated Glut4 trafficking to the plasma membrane via the exocyst and the motor protein Myo1c. Dev Cell 13, 391–404.

Chiu TT, Jensen TE, Sylow L, Richter EA, Klip A (2011a). Rac1 signalling towards GLUT4/glucose uptake in skeletal muscle. Cell Signal 23, 1546–1554.

Chiu TT, Patel N, Shaw AE, Bamburg JR, Klip A (2011b). Arp2/3- and cofilin-coordinated actin dynamics is required for insulin-mediated GLUT4 translocation to the surface of muscle cells. Mol Biol Cell 21, 3529–3539.

Chung Le TK, Hosaka T, Harada N, Jambaldorj B, Fukunaga K, Nishiwaki Y, Teshigawara K, Sakai T, Nakaya Y, Funaki M (2009). Myosin IIA participates in docking of Glut4 storage vesicles with the plasma membrane in 3T3-L1 adipocytes. Biochem Biophys Res Commun 391, 995–999.

Ciccone MA, Timmons M, Phillips A, Quick MW (2008). Calcium/calmodulin-dependent kinase II regulates the interaction between the serotonin transporter and syntaxin 1A. Neuropharmacology 55, 763–770.

Coultrap SJ, Buard I, Kulbe JR, Dell'Acqua ML, Bayer KU (2010). CaMKII autonomy is substrate-dependent and further stimulated by Ca^{2+}/calmodulin. J Biol Chem 285, 17930–17937.

DiFranco M, Quinonez M, Capote J, Vergara J (2009). DNA transfection of mammalian skeletal muscles using in vivo electroporation. J Vis Exp 32, 1520.

Dugani CB, Klip A (2005). Glucose transporter 4: cycling, compartments and controversies. EMBO Rep 6, 1137–1142.

Dugani CB, Randhawa VK, Cheng AW, Patel N, Klip A (2008). Selective regulation of the perinuclear distribution of glucose transporter 4 (GLUT4) by insulin signals in muscle cells. Eur J Cell Biol 87, 337–351.

Egea G, Lazaro-Dieguez F, Vilella M (2006). Actin dynamics at the Golgi complex in mammalian cells. Curr Opin Cell Biol 18, 168–178.

Evangelista M, Klebl BM, Tong AH, Webb BA, Leeuw T, Leberer E, Whiteway M, Thomas DY, Boone C (2000). A role for myosin-I in actin assembly through interactions with Vrp1p, Bee1p, and the Arp2/3 complex. J Cell Biol 148, 353–362.

Foley K, Boguslavsky S, Klip A (2011). Endocytosis, recycling, and regulated exocytosis of glucose transporter 4. Biochemistry 50, 3048–3061.

Foster LJ, Klip A (2000). Mechanism and regulation of GLUT-4 vesicle fusion in muscle and fat cells. Am J Physiol Cell Physiol 279, C877–C890.

Foster LJ, Rudich A, Talior I, Patel N, Huang X, Furtado LM, Bilan PJ, Mann M, Klip A (2006). Insulin-dependent interactions of proteins with GLUT4 revealed through stable isotope labeling by amino acids in cell culture (SILAC). J Proteome Res 5, 64–75.

Frantz C, Barreiro G, Dominguez L, Chen X, Eddy R, Condeelis J, Kelly MJ, Jacobson MP, Barber DL (2008). Cofilin is a pH sensor for actin free barbed end formation: role of phosphoinositide binding. J Cell Biol 183, 865–879.

Hagan GN, Lin Y, Magnuson MA, Avruch J, Czech MP (2008). A Rictor-Myo1c complex participates in dynamic cortical actin events in 3T3-L1 adipocytes. Mol Cell Biol 28, 4215–4226.

Hokanson DE, Laakso JM, Lin T, Sept D, Ostap EM (2006). Myo1c binds phosphoinositides through a putative pleckstrin homology domain. Mol Biol Cell 17, 4856–4865.

Ishida A, Kameshita I, Okuno S, Kitani T, Fujisawa H (1995). A novel highly specific and potent inhibitor of calmodulin-dependent protein kinase II. Biochem Biophys Res Commun 212, 806–812.

Ishikura S, Klip A (2008). Muscle cells engage Rab8A and myosin Vb in insulin-dependent GLUT4 translocation. Am J Physiol Cell Physiol 295, C1016–1025.

Ishikura S, Koshkina A, Klip A (2008). Small G proteins in insulin action: Rab and Rho families at the crossroads of signal transduction and GLUT4 vesicle traffic. Acta Physiol (Oxf) 192, 61–74.

JeBailey L, Rudich A, Huang X, Di Ciano-Oliveira C, Kapus A, Klip A (2004). Skeletal muscle cells and adipocytes differ in their reliance on TC10 and Rac for insulin-induced actin remodeling. Mol Endocrinol 18, 359–372.

JeBailey L, Wanono O, Niu W, Roessler J, Rudich A, Klip A (2007). Ceramide- and oxidant-induced insulin resistance involve loss of insulin-dependent Rac-activation and actin remodeling in muscle cells. Diabetes 56, 394–403.

Kanzaki M, Pessin JE (2001). Insulin-stimulated GLUT4 translocation in adipocytes is dependent upon cortical actin remodeling. J Biol Chem 276, 42436–42444.

Khayat ZA, Tong P, Yaworsky K, Bloch RJ, Klip A (2000). Insulin-induced actin filament remodeling colocalizes actin with phosphatidylinositol 3-kinase and GLUT4 in L6 myotubes. J Cell Sci 113, 279–290.

Koivusalo M, Welch C, Hayashi H, Scott CC, Kim M, Alexander T, Touret N, Hahn KM, Grinstein S (2010). Amiloride inhibits macropinocytosis by lowering submembranous pH and preventing Rac1 and Cdc42 signaling. J Cell Biol 188, 547–563.

Kolarow R, Brigadski T, Lessmann V (2007). Postsynaptic secretion of BDNF and NT-3 from hippocampal neurons depends on calcium calmodulin kinase II signaling and proceeds via delayed fusion pore opening. J Neurosci 27, 10350–10364.

Lanzetti L (2007). Actin in membrane trafficking. Curr Opin Cell Biol 19, 453–458.

Lechler T, Shevchenko A, Li R (2000). Direct involvement of yeast type I myosins in Cdc42-dependent actin polymerization. J Cell Biol 148, 363–373.

Lizunov V, Stenkula K, Lisinski I, Gavrilova O, Yver DR, Chadt A, Al-Hasani H, Zimmerberg J, Cushman SW (2012). Insulin stimulates fusion, but not

tethering, of GLUT4 vesicles in skeletal muscle of transgenic mouse. Am J Physiol Endocrinol Metab 2012, 31.
Lopez JA, Burchfield JG, Blair DH, Mele K, Ng Y, Vallotton P, James DE, Hughes WE (2009). Identification of a distal GLUT4 trafficking event controlled by actin polymerization. Mol Biol Cell 20, 3918–3929.
Loubery S, Coudrier E (2008). Myosins in the secretory pathway: tethers or transporters. Cell Mol Life Sci 65, 2790–2800.
McConnell RE, Tyska MJ (2010). Leveraging the membrane—cytoskeleton interface with myosin-1. Trends Cell Biol 20, 418–426.
McKenna JM, Ostap EM (2009). Kinetics of the interaction of myo1c with phosphoinositides. J Biol Chem 284, 28650–28659.
Nambiar R, McConnell RE, Tyska MJ (2009). Control of cell membrane tension by myosin-I. Proc Natl Acad Sci USA 106, 11972–11977.
Nascimento AA, Roland JT, Gelfand VI (2003). Pigment cells: a model for the study of organelle transport. Annu Rev Cell Dev Biol 19, 469–491.
Patel N, Rudich A, Khayat ZA, Garg R, Klip A (2003). Intracellular segregation of phosphatidylinositol-3,4,5-trisphosphate by insulin-dependent actin remodeling in L6 skeletal muscle cells. Mol Cell Biol 23, 4611–4626.
Pollard TD (2007). Regulation of actin filament assembly by Arp2/3 complex and formins. Annu Rev Biophys Biomol Struct 36, 451–477.
Ramm G, Slot JW, James DE, Stoorvogel W (2000). Insulin recruits GLUT4 from specialized VAMP2-carrying vesicles as well as from the dynamic endosomal/trans-Golgi network in rat adipocytes. Mol Biol Cell 11, 4079–4091.
Randhawa VK, Ishikura S, Talior-Volodarsky I, Cheng AW, Patel N, Hartwig JH, Klip A (2008). GLUT4 vesicle recruitment and fusion are differentially regulated by Rac, AS160, and Rab8A in muscle cells. J Biol Chem 283, 27208–27219.
Randhawa VK, Thong FS, Lim DY, Li D, Garg RR, Rudge R, Galli T, Rudich A, Klip A (2004). Insulin and hypertonicity recruit GLUT4 to the plasma membrane of muscle cells by using *N*-ethylmaleimide-sensitive factor-dependent SNARE mechanisms but different v-SNAREs: role of TI-VAMP. Mol Biol Cell 15, 5565–5573.
Reizes O, Barylko B, Li C, Sudhof TC, Albanesi JP (1994). Domain structure of a mammalian myosin Iβ. Proc Natl Acad Sci USA 91, 6349–6353.
Ridley AJ (2006). Rho GTPases and actin dynamics in membrane protrusions and vesicle trafficking. Trends Cell Biol 16, 522–529.
Sokac AM, Schietroma C, Gundersen CB, Bement WM (2006). Myosin-1c couples assembling actin to membranes to drive compensatory endocytosis. Dev Cell 11, 629–640.
Stockli J, Fazakerley DJ, James DE (2012). GLUT4 exocytosis. J Cell Sci 124, 4147–4159.
Talior-Volodarsky I, Randhawa VK, Zaid H, Klip A (2008). α-Actinin-4 is selectively required for insulin-induced GLUT4 translocation. J Biol Chem 283, 25115–25123.
Tamrakar AK, Schertzer JD, Chiu TT, Foley KP, Bilan PJ, Philpott DJ, Klip A (2011). NOD2 activation induces muscle cell-autonomous innate immune responses and insulin resistance. Endocrinology 151, 5624–5637.
Tang N, Lin T, Ostap EM (2002). Dynamics of myo1c (myosin-Iβ) lipid binding and dissociation. J Biol Chem 277, 42763–42768.
Thomann D, Rines DR, Sorger PK, Danuser G (2002). Automatic fluorescent tag detection in 3D with super-resolution: application to the analysis of chromosome movement. J Microsc 208, 49–64.
Tokumitsu H, Chijiwa T, Hagiwara M, Mizutani A, Terasawa M, Hidaka H (1990). KN-62, 1-[N,O-bis(5-isoquinolinesulfonyl)-N-methyl-L-tyrosyl]-4-phenylpiperazine, a specific inhibitor of Ca^{2+}/calmodulin-dependent protein kinase II. J Biol Chem 265, 4315–4320.
Tong P, Khayat ZA, Huang C, Patel N, Ueyama A, Klip A (2001). Insulin-induced cortical actin remodeling promotes GLUT4 insertion at muscle cell membrane ruffles. J Clin Invest 108, 371–381.
Torok D, Patel N, Jebailey L, Thong FS, Randhawa VK, Klip A, Rudich A (2004). Insulin but not PDGF relies on actin remodeling and on VAMP2 for GLUT4 translocation in myoblasts. J Cell Sci 117, 5447–5455.
Toyoda T, An D, Witczak CA, Koh HJ, Hirshman MF, Fujii N, Goodyear LJ (2011). Myo1c regulates glucose uptake in mouse skeletal muscle. J Biol Chem 286, 4133–4140.
Tsakiridis T, Vranic M, Klip A (1994). Disassembly of the actin network inhibits insulin-dependent stimulation of glucose transport and prevents recruitment of glucose transporters to the plasma membrane. J Biol Chem 269, 29934–29942.
Ueyama A, Yaworsky KL, Wang Q, Ebina Y, Klip A (1999). GLUT-4myc ectopic expression in L6 myoblasts generates a GLUT-4-specific pool conferring insulin sensitivity. Am J Physiol 277, E572–E578.
Vest RS, Davies KD, O'Leary H, Port JD, Bayer KU (2007). Dual mechanism of a natural CaMKII inhibitor. Mol Biol Cell 18, 5024–5033.
Watson RT, Pessin JE (2007). GLUT4 translocation: the last 200 nanometers. Cell Signal 19, 2209–2217.
Williams D, Pessin JE (2008). Mapping of R-SNARE function at distinct intracellular GLUT4 trafficking steps in adipocytes. J Cell Biol 180, 375–387.
Witczak CA, Jessen N, Warro DM, Toyoda T, Fujii N, Anderson ME, Hirshman MF, Goodyear LJ (2010). CaMKII regulates contraction- but not insulin-induced glucose uptake in mouse skeletal muscle. Am J Physiol Endocrinol Metab 298, E1150–E1160.
Xu Y, Rubin BR, Orme CM, Karpikov A, Yu C, Bogan JS, Toomre DK (2011). Dual-mode of insulin action controls GLUT4 vesicle exocytosis. J Cell Biol 193, 643–653.
Yip MF, Ramm G, Larance M, Hoehn KL, Wagner MC, Guilhaus M, James DE (2008). CaMKII-mediated phosphorylation of the myosin motor Myo1c is required for insulin-stimulated GLUT4 translocation in adipocytes. Cell Metab 8, 384–398.
Yoshizaki T, Imamura T, Babendure JL, Lu JC, Sonoda N, Olefsky JM (2007). Myosin 5a is an insulin-stimulated Akt2 (protein kinase Bβ) substrate modulating GLUT4 vesicle translocation. Mol Cell Biol 27, 5172–5183.
Zaid H, Antonescu CN, Randhawa VK, Klip A (2008). Insulin action on glucose transporters through molecular switches, tracks and tethers. Biochem J 413, 201–215.